O^- bound small polarons in oxide materials

2006 J. Phys.: Condens. Matter 18 R667

(http://iopscience.iop.org/0953-8984/18/43/R01)

INSTITUTE OF PHYSICS PUBLISHING JOURNAL OF PHYSICS: CONDENSED MATTER

J. Phys.: Condens. Matter **18** (2006) R667–R704 doi:10.1088/0953-8984/18/43/R01

TOPICAL REVIEW

O^- bound small polarons in oxide materials

O F Schirmer

Department of Physics, University of Osnabrück, D-49076 Osnabrück, Germany

E-mail: schirmer@uos.de

Received 14 June 2006, in final form 12 September 2006
Published 13 October 2006
Online at stacks.iop.org/JPhysCM/18/R667

Abstract

Holes bound to acceptor defects in oxide crystals are often localized by lattice distortion at just one of the equivalent oxygen ligands of the defect. Such holes thus form small polarons in symmetric clusters of a few oxygen ions. An overview on mainly the optical manifestations of those clusters is given. The article is essentially divided into two parts: the first one covers the basic features of the phenomena and their explanations, exemplified by several paradigmatic defects; in the second part numerous oxide materials are presented which exhibit bound small polaron optical properties. The first part starts with summaries on the production of bound hole polarons and the identification of their structure. It is demonstrated why they show strong, wide absorption bands, usually visible, based on polaron stabilization energies of typically 1 eV. The basic absorption process is detailed with a fictitious two-well system. Clusters with four, six and twelve equivalent ions are realized in various oxide compounds. In these cases several degenerate optically excited polaron states occur, leading to characteristic final state resonance splittings. The peak energies of the absorption bands as well as the sign of the transfer energy depend on the topology of the clusters. A special section is devoted to the distinction between interpolaron and intrapolaron optical transitions. The latter are usually comparatively weak. The oxide compounds exhibiting bound hole small polaron absorptions include the alkaline earth oxides (e.g. MgO), BeO and ZnO, the perovskites $BaTiO_3$ and $KTaO_3$, quartz, the sillenites (e.g. $Bi_{12}TiO_{20}$), Al_2O_3, $LiNbO_3$, topaz and various other materials. There are indications that the magnetic crystals NiO, doped with Li, and $LaMnO_3$, doped with Sr, also show optical features caused by bound hole polarons. Beyond being elementary paradigms for the properties of small polarons in general, the defect species treated can be used to explain radiation and light induced absorption especially in laser and non-linear oxide materials, the role of some defects in photorefractive compounds, the coloration of various gemstones, the structure of certain catalytic surface centres, etc. The relation to further phenomena is discussed: free small polarons, similar distorted centres in the sulfides and selenides, acceptor defects trapping two holes.

(Some figures in this article are in colour only in the electronic version)

Contents

1. Introduction

Valence band holes in oxide materials tend to be trapped at negatively charged acceptor defects. Examples are provided by transition metal or rare earth ions with lower valencies than the replaced cations, but also cation vacancies and simple ions, such as Li^+, Mg^{2+}, Al^{3+} etc. In the latter cases, the electron ionization energies are high and a hole will thus be captured at the neighbouring oxygen ions rather than at the defect itself. In crystalline matter there are usually several equivalent oxygen sites surrounding a point defect. Cases of tetrahedral symmetry, with four equivalent oxygen sites, and with octahedral symmetry, comprising either six or twelve equivalent sites, have been investigated.

In spite of the equivalence of the oxygen ions in such clusters, in most cases it turns out that hole–lattice coupling favours hole localization at a single one among them, forming an isolated O^- ion. This is caused by lattice distortion, breaking the point group symmetry. It is thus useful to label such defects as small polarons, bound to an acceptor. This nomenclature stresses the analogy to free small polarons in ideal lattices, where the space group symmetry can be broken by localization of a charge carrier at one of numerous equivalent sites, also induced by coupling to the lattice. For small polarons the carrier is essentially restricted to one site and the distortion mainly involves the bonds to its first neighbours. By polarons this article will always mean small ones and the term 'small' will only be added if clarity requires it. For an overview on the various kinds of polarons in general, emphasizing their optical properties, see Emin [1]. Also the numerical treatment of the optical properties of various manifestations of polarons by Alexandrov *et al* [2] may be consulted.

The lattice distortion stabilizing a polaron is counteracted by tunnelling, which is facilitated by the equivalence of the sites concerned. The eigenstates of this symmetry restoring interaction are molecular orbitals having appropriately phased amplitudes at the equivalent oxygen ions. These states usually are not degenerate, and interaction with the lattice can thus be termed a pseudo-Jahn–Teller effect. This point group situation again is analogous to the space group case. There the tunnelling leads to nearly degenerate Bloch states and lattice interaction has to cope with the corresponding lack of degeneracy. For the ground states of strongly localized polarons, however, tunnelling is only a small, but decisive perturbation. Details will be mentioned below.

It turns out that these simple systems, single O^- ions next to acceptor defects in oxide systems, have a series of intriguing aspects, as regards their electronic and ionic structure as well as their optical features, the methods of their investigation and their roles in various applications of oxide materials. This review will collect the experience gained with such polarons which has cumulated during the last few decades. It will also show how the model of bound O^- polarons was successfully applied more recently to new classes of compounds, explaining related phenomena in a series of optical and other materials. First a heuristic introduction to the electronic structure of the centres will be given, starting from a simple—albeit fictitious—system of two equivalent oxygen ions, each equally likely to capture a hole. This paradigm allows one to deduce the essential features of the systems, such as the influence of lattice coupling on their energy levels and the consequences for optically induced site changes of an O^- hole. These results turn out to be a guide for the assessment of small polaron features in general. Since the strong optical absorption caused by the light induced charge transfer between both oxygen sites is their most conspicuous directly accessible characteristic, the main emphasis will be on the optical processes connected with bound O^- polarons. Next, O^- centres containing four, six and twelve equivalent oxygen ions will be treated and the strong dependence of the peak energies of the polaron bands on the topology will be pointed out and explained. A feature characteristic for such systems is a resonance splitting of the excited states in the distorted geometry, giving characteristic fingerprints of their optical spectra.

Up to this stage all oxygen ions involved are assumed to be equivalent. The generalization to systems with slightly inequivalent ions up to strongly different ones will also be discussed. The underlying optical charge transfer mechanism also prevails in these cases, even if the transition probability is attenuated by the energy difference between the hole ground states at the related sites.

This overview intends to introduce to the various optical manifestations of O^- bound polarons in numerous materials under common guidelines. To this end the most concise and flexible relevant theoretical approach is chosen, a scheme involving a single configurational coordinate, similar to that known from many studies of colour centres, where the carrier density is centred around one site. The modifications necessary for the special situation of polarons, i.e. charge carriers potentially present in equivalent states at more than one site, will be introduced. In this way a middle course is followed. It is distinguished, on one side, from a detailed consideration of all degrees of freedom of a lattice interacting with a carrier. Approaches of this type initially led to the elucidation of the optical properties of free small polarons by Reik [3], Klinger [4] and Reik and Heese [5]. On the other side, there are increasing successes in predicting the optical properties of, e.g., bound O^- polarons by detailed quantum chemical investigations (see e.g. Norgett *et al* [6], To *et al* [7]), which tend to emphasize the peculiarities of the specific systems studied; they can lead to a direct theoretical determination of the parameters obtained by fitting to experimental data in the former two phenomenological approaches. Polarons as seen mainly from the viewpoint of their atomistic simulations have been treated by Shluger and Stoneham [8].

The term 'bound small polaron' has previously also been applied (see, e.g., Calvani [9]) to carriers trapped at the single site of a defect and stabilized there by lattice distortion, i.e. following the traditional colour centre concept. When designating the present objects as bound polarons we stress the close relationship to free small polarons, able to 'choose' among all, in principle, equivalent sites in a crystal. The study of bound polarons of the present type thus allows one to gain insight also into the usually more involved features of free small polarons.

On the experimental side, numerous methods have been used to elucidate the properties of the O^- systems. For crystals with non-magnetic host lattice cations, basic knowledge on their electronic and geometric structure always results from studies of electron paramagnetic resonance (EPR), augmented by optically detected magnetic resonance (ODMR) and the study of light induced optical absorption changes. These tie the strong optical absorptions to usually well-established microscopic models. The EPR parameters of many O^- defects are known; we refrain from giving a complete list of these results but rather concentrate on those cases for which hole localization at one oxygen site is established and where data on correlated optical absorption features are available.

The detailed experimental information on the structure of the defects represents a fixed basis on which the theoretical interpretation of the optical absorptions must rely. This situation is not always fulfilled for the case for free small polarons, and the interpretations of their optical properties sometimes have to be based solely on the consistency of arguments about their optical absorption. As a further difference it should be mentioned that optical absorptions of bound O^- polarons lie at energies in the visible and nearby, whereas free small polarons tend to absorb in the near infrared and at lower energies. This difference is caused, in essence, by the larger stabilization energies of bound hole polarons, typically around 1 eV, to be compared with values around 0.2–0.5 eV for free ones. An excellent overview on the optical properties of free polarons has been presented recently by Calvani [9].

Since O^- hole polarons are most frequently produced optically, it is not astonishing that they occur often in materials whose function is characterized by interaction with intense light, such as laser crystals, electro-optic and especially non-linear optic materials, among them also photorefractive ones. But O^- bound polarons are also found outside of these categories, and the first detailed studies of bound hole polarons have been performed with simple oxides, such as MgO and related compounds.

The list of compounds in which optical effects of O^- centres have been identified so far comprises the following substances (also in variously doped modifications): MgO, CaO; BeO, ZnO; Al_2O_3; $YAlO_3$; $BaTiO_3$, $KTaO_3$; $KTiOPO_4$, α-quartz; $Bi_{12}MO_{20}$ (M = Ti or Si or Ge), etc. Also NiO:Li and $LaMnO_3$:Sr show indications of bound O^--type optical absorption. Similar phenomena are also met in the sulfides and selenides.

This review is organized as follows. It will start with some information on the preparation of the polarons and their experimental analysis. An outline of the analysis of their optical absorption features will follow, concentrating first on oxygen–acceptor clusters with high symmetry, comprising between two and twelve symmetrically arranged oxygen ions. With this background knowledge it is easier to give a summary of the distinction between intrapolaron and interpolaron transitions. Then a series of further incidences of hole polaron optical absorptions will be presented. In a concluding section several fields of research, which have features in common with the present topic, will be touched on.

2. Production of O^- bound polarons and the methods of their investigation

2.1. Production

The holes to be trapped at acceptor defects are created by chemical or optical doping. The latter procedure is used predominantly. Usually electrons are excited from the valence to the

conduction band or to defects having gap levels, forming valence band holes. Less frequently also a direct optical ionization of O^{2-} ions next to an acceptor to the conduction band takes place. These excitation processes can be caused by the absorption of one or more photons or the secondary radiation effects following x-ray, electron or neutron irradiation. Since the created situations represent deviations from the crystal ground states, they are not stable and eventually the holes will recombine with the electrons separated from them. Such electrons are often accommodated at levels near to the conduction band edge. The lifetime of the hole states, with which we are concerned, is determined by the shallower of the two species, trapped electron or hole. In high gap materials, such as quartz, the hole lifetimes can still be effectively infinite at room temperature as exemplified by holes next to Al_{Si}^{3+}, caused by the radioactivity at the geological deposit of quartz. The O^- next to Al^{3+} can be at least partly responsible for the smoky coloration of quartz.

A strong chemical doping with acceptor defects can lead to spontaneous compensation by holes, without further illumination. In such a case, the Fermi level is stabilized at the acceptor level and partially filled acceptor states occur. Sometimes, however, an additional heat treatment in an oxygen atmosphere is necessary for removing competing intrinsic positive defects, such as oxygen vacancies, in order to achieve this situation. This is known to take place, e.g., for Al_2O_3 doped with Mg [10], and the hole concentration increases strongly with rising oxygen partial pressure.

2.2. Electron paramagnetic resonance

O^- ions next to acceptor sites have rather unique magnetic fingerprints, allowing one to prove their presence as well as to identify the underlying microscopic structure of the related defects by using electron paramagnetic resonance (EPR), at least in crystals with non-magnetic cations. A few remarks are given on how the orbital structure of the ground states is determined in this way. An O^- ion is paramagnetic, since one electron is missing in the oxygen 2p shell. In the non-cubic environments of such ions, either present in the unperturbed crystal already or caused by association with defects together with the accompanying lattice distortion, the coupling of the $S = 1/2$ spin to the 2p orbital ($L = 1$) is weak in most cases, leading to rather long spin–lattice relaxation times. This allows EPR investigations to be performed sometimes even at 300 K. Zeeman interaction with an external static magnetic field, $\boldsymbol{B}$, and hyperfine coupling with magnetic nuclei within the range of finite hole amplitudes determine the structure of EPR spectra of such O^- systems.

The structure of the g-tensors, describing the Zeeman interaction, is given for a singly degenerate orbital by

$$g_{ij} = g_s - \Delta g_{ij} = g_s - 2\lambda \sum_n \frac{\langle 0|L_i|n\rangle\langle n|L_j|0\rangle}{E_n - E_0} \tag{1}$$

(see, e.g., [11]; λ the spin–orbit coupling constant of O^-, L_i the operator of orbital angular momentum, n and 0 label excited state n and the ground state, respectively). This indicates that there is no first-order orbital contribution to g_{ij}. The perturbation terms in equation (1) follow from the combined influence of spin–orbit ($\lambda \boldsymbol{LS}$) and orbit–Zeeman ($\boldsymbol{BL}$) interaction. If the magnetic field $\boldsymbol{B}$ is oriented along the axis of a ground state 2p lobe, as for p_z in figure 1(a), only the orbital operator L_z is active. But since $L_z|p_z\rangle = 0$, the corresponding matrix elements are zero and $\Delta g \approx 0$ is measured along such directions; this allows one to identify the direction of a ground state p lobe. Because the positive hole is attracted by the negative acceptor, the situation of figure 1(a) is met usually. If, however, the sign of the crystal field is inverted, as e.g. for the oxygen sites in α-quartz or in some oxide perovskites, the configuration of figure 1(b) is found,

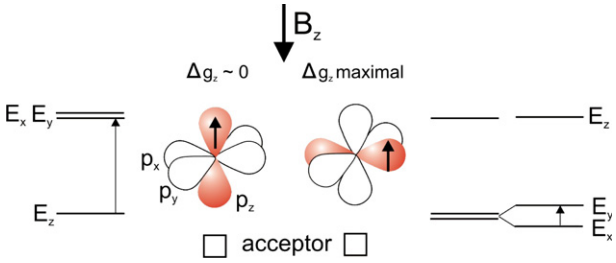

Figure 1. Orbital structure of O^- next to an acceptor site, defining an axis, and the g-shifts expected for $\boldsymbol{B}$ along this axis. Left, (a): the σ-type ground state p lobe is oriented along the axis. Along the direction of the p_z lobe $\Delta g \sim 0$ is measured. Right, (b): for an inverted crystal field, not dominated by the acceptor charge, a π-type ground state, with lobes perpendicular to the axis, is found. This is the case, e.g., for the non-bonding oxygen orbitals in SiO_2 or the ABO_3 perovskites with highly charged B cations. Here the largest possible deviation of g from the free spin value g_s is measured if $\boldsymbol{B}$ is oriented along the axis, z. The small energy difference from the ground state to the next orbital level indicated is responsible for this. For $\boldsymbol{B}$ along the p_x lobe, again $\Delta g \sim 0$ is measured.

where the axis of the ground state 2p lobe is perpendicular to the axis of the defect. Here $\Delta g \approx 0$ is measured along p_x and a maximal deviation of g from g_s, typically of the order up to 0.1, now occurs for $\boldsymbol{B}$ along the axis of the centre. This is caused by the near degeneracy of the two lowest orbitals. In perfect axial symmetry they would be completely degenerate, but then a Jahn–Teller effect occurs, introducing a slight orthorhombicity. Recently the peculiar spectroscopic fingerprints have been derived for the special situation [12] where the Jahn–Teller effect in such a situation is not static, as shown in figure 1(b), but dynamic.

There are cases where no direction of $\boldsymbol{B}$ can be found for which Δg is close to zero. Among other models, such situations can point to the fact that an O^- hole is delocalized over two neighbouring oxygen ions, as e.g. for a hole next to Al^{3+} in $BaTiO_3$ [13, 14]. Such cases, however, occur rather seldom for oxides.

Hyperfine coupling can yield information, in favourable cases, on the chemical identity of the interacting nuclei and their distances to the O^- ion, as well as the spin densities of the hole wavefunction at the nuclear sites. In the case where the interacting nuclei have spin $I \geqslant 1$, quadrupole coupling can be used to inform us about the local electric field gradients. If quantum mechanical models can be found, which consistently reproduce all experimental findings, they may be taken as a reliable mirror of the underlying defect. Once a model has been 'solved' in this way, it is possible to calculate the matrix elements in equation (1) and then the energy denominators, i.e. estimates of the energy distances to the excited 2p crystal field states can be derived, if the spin–orbit coupling parameter of O^- ($\lambda \sim 135\ cm^{-1}$) is inserted.

2.3. Optical absorption

There are several methods for identifying the absorption features caused by O^- defects, as established by EPR studies. The most compelling one is the use of ODMR (optically detected magnetic resonance; see e.g. Spaeth *et al* [15]). For applications to absorption signals, the magnetic circular dichroism (MCD) occurring in a static magnetic field is exploited. In general, a part of this MCD is caused by the population difference of the Zeeman sublevels of the ground state, from which absorptions by right and left circularly polarized transitions start. If the sublevel populations are changed by the corresponding magnetic resonance transitions, the MCD signals will vary accordingly, reflecting the EPR spectra of the ground state. In this way

the EPR, with all its information on the defect structure, is monitored via the related optical features themselves. The earliest measurements of this type on O^- defects were performed by Izen, Mazo and Kemp with O^- holes next to a Mg vacancy in MgO [16]. References to newer work, also concerning other O^- defects, will be given below.

A further merit of ODMR studies using MCD is worth mentioning. Since the method is highly specific for optical transitions originating at the ground state of a given paramagnetic object, this ODMR can be used to discriminate from possibly superimposed absorption features starting from ground states of other defect centres.

Another method correlating defect structure and optical absorption exploits the photochromicity, i.e. the light induced optical absorption changes connected with the creation of O^- defects, for instance by illumination, as mentioned above. If the dependence of this photochromicity on the rising energy of the exciting light correlates with the changes of the EPR of O^-, monitored simultaneously, a necessary condition is fulfilled that the two features, optical absorption and EPR of O^-, are connected to each other. This technique has recently been realized with instrumentation specially developed for this purpose [17]. Since the optical absorption changes can result from all defects in a material involved in a recharging process under illumination, the method allows one to give a rather complete overview on the scenario of the light induced charge transpositions in a material.

In principle any variation of external conditions, simultaneously affecting optical absorption and EPR, can identify such correlations. Under the description 'isochronic annealing', i.e. by definite heating of a sample previously optically excited at low temperatures, several O^- absorption bands have been identified. Also the changes of absorption spectra and their polarizations under an applied electric field have been used to identify O^- defects [18], for which innate electric dipole moments are characteristic. Sometimes, only the simultaneous occurrence of typical optical absorption bands and EPR of O^- have led to a corresponding assignment. From all these studies, it turns out that O^- defects cause rather wide, intense Gaussian-type bands, with absorption features often in the visible spectral range. They thus can be rather potent colour centres.

Related is the study of the dielectric relaxation and absorption connected with the electric moments of the acceptor—O^- dipoles. Since these are necessarily accompanied by their elastic analogues, elastic dipoles, it is not astonishing that some O^- defects were studied using ultrasound attenuation (e.g. [19, 20]).

3. Hole polarons in point symmetric clusters and their optical absorption

3.1. Two-well system

A hole trapped at one of two O^{2-} ions, having equivalent positions with respect to a capturing defect, is the simplest conceivable model for bound O^- polarons. We use this scheme to introduce their main features, although such a situation does not exist in reality to our knowledge. The somewhat more complicated cases of four, six, and twelve equivalent sites, identified experimentally, are based on this introductory example. Figure 2 depicts the situation: a hole can be located at the left or right of a trapping defect. If transfer between the two sites is admitted, a splitting into symmetric and antisymmetric states is expected.

The system can couple to an asymmetric mode of the two-site vibrations, modelling the main influence of the surrounding lattice which is of interest in the present context. This interaction leads to the level scheme showing the total energies in the space of the configuration coordinate of the vibration, Q. The coupling between the hole and the vibration system is

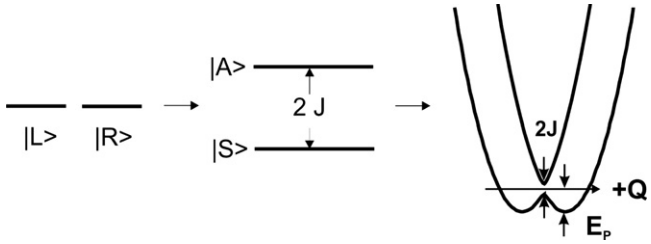

Figure 2. A carrier potentially present at one of two sites (left), equivalent with respect to a capturing defect (not shown), can be transferred between the two positions, leading to the resonance split states indicated in the middle. Coupling to an asymmetric vibration, configuration coordinate Q, causes a stabilization, E_P, of the carrier–vibration system as indicated on the right.

expressed by

$$H = -J\begin{pmatrix}1 & 0\\ 0 & -1\end{pmatrix} + VQ\begin{pmatrix}0 & 1\\ 1 & 0\end{pmatrix} + S\begin{pmatrix}1 & 0\\ 0 & 1\end{pmatrix} \qquad \text{operating on the basis } \begin{pmatrix}S\\ A\end{pmatrix}. \quad (2)$$

J is the transfer energy, V the strength of the coupling to the vibration and $S = (1/2)(\mu\omega_0^2 Q^2 + (1/\mu)P^2)$ the Hamiltonian of the vibration, with standard notation.

Alternatively, the problem can be formulated in the basis $\begin{pmatrix}\mathrm{L}\\ \mathrm{R}\end{pmatrix}$:

$$H = \begin{pmatrix}VQ + S & J\\ J & -VQ + S\end{pmatrix}. \quad (3)$$

Concentrating on the essential features of the problem, the non-zero overlap between the states centred at the left and the right is neglected when calculating the eigenvalues of H. The graph on the right in figure 2 results in both approaches; only the elastic energy of the vibration is considered, i.e. the static case ($P = 0$) is taken. Assuming that the hole is localized at one of the equivalent sites, representative for most cases identified experimentally, the transfer energy can be taken as a perturbation. Then the second approach is more useful.

It is seen that the coupling decreases the energy of the hole–vibration system by

$$E_P = V^2/4K \qquad \text{with } K = (1/2)\mu\omega_0^2 \text{ at the equilibrium distortions } Q_{\min} = \pm V/2K. \quad (4)$$

We are concerned with the optical absorption of bound small polarons and will discuss this on the basis of a procedure similar to that familiar for colour centres with a charge carrier bound at one site by Coulomb attraction and lattice distortion [21]. Here ground and excited states are determined by the Coulomb potential and the corresponding couplings to the lattice. For small polarons two modifications are required, since they can be localized at two or more ions: first, because of the equivalence of the sites involved there is no energy difference of the initial and final electronic states, in contrast to the situation usually found for colour centres. All energy differences between the potentials in figure 2 result only from coupling to the lattice. Second, the initial and final electronic states are not orthogonal to each other and the resulting mixing between the two states allows the occurrence of charge transfer transitions between neighbouring sites.

The transition rate, T, for allowed optical transitions from the state at the lower sheet, Ψ_L (left in figure 3), to that of the upper one, Ψ_R, at a given distortion Q is proportional to the square of the electric dipole matrix element:

$$T \propto |\langle \Psi_L | e\vec{r} | \Psi_R \rangle|^2. \quad (5)$$

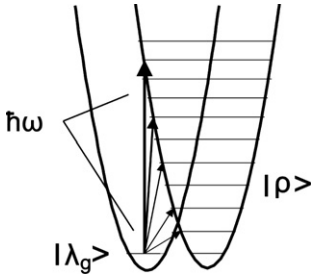

Figure 3. Features of a two-well system essential in the present context. The left well corresponds to the initial state.

Using the adiabatic approximation, $\Psi_{\mathrm{L}} = |\mathrm{L}'\rangle|\lambda\rangle$ and $\Psi_{\mathrm{R}} = |\mathrm{R}'\rangle|\rho\rangle$, where the electronic parts, $|\mathrm{L}'\rangle$ and $|\mathrm{R}'\rangle$, will be detailed below, this can be broken down into its electronic and vibrational components:

$$T \propto |\langle \mathrm{L}'|e\vec{r}|\mathrm{R}'\rangle|^2 |\langle \lambda_{\mathrm{g}}|\rho\rangle|^2. \tag{6}$$

For simplicity, temperature zero will be assumed, implying that only the lowest vibrational level at the left well, λ_{g}, is occupied (figure 3).

The electronic part is considered first. Treating the off-diagonal elements J in equation (3) in first order, it is found that

$$|\mathrm{L}'\rangle = |\mathrm{L}\rangle + (J/\Delta E)|\mathrm{R}\rangle \qquad \text{and} \qquad |\mathrm{R}'\rangle = |\mathrm{R}\rangle - (J/\Delta E)|\mathrm{L}\rangle \tag{7}$$

where ΔE is the difference between the diagonal elements in equation (3), i.e. the energy distance between the lower and upper sheets in figure 3. For the classical boundary case, this energy difference is also the energy of the absorbed photon, $\Delta E \sim h\omega$.

Calculating the expectation value $\vec{l} = \langle \mathrm{L}'|\vec{r}|\mathrm{R}'\rangle$ of the transition vector with the first-order perturbed states (equation (7)), one arrives at

$$\vec{l} \approx (J/\hbar\omega)\vec{d} \tag{8}$$

where $\vec{d}$ is the vector between the left and right sites. The energy absorption rate, $\hbar\omega * T$, is thus proportional to $(Jd)^2/\hbar\omega$, with d the length of $\vec{d}$. This estimate of the first part in equation (6) gives the dependence of the intensity of the small polaron absorption on the indicated parameters. The exact theory, analytically formulated for the optical behaviour of free small polarons [2–4], leads to identical behaviour with respect to the dependence on J, d and ω.

As is known, the second factor in equation (6) describes the shape of the absorption band. This square of the projection of the vibrational ground state $|\lambda_{\mathrm{g}}\rangle$ on the nth vibrational state on the right, $|\rho_n\rangle$, is

$$|\langle \lambda_{\mathrm{g}}|\rho_n\rangle|^2 = \frac{S^n \exp(-S)}{n!} \tag{9}$$

describing the relative intensities of the related vibrational transitions, with the Huang–Rhys factor $S = 4E_{\mathrm{p}}/\hbar\omega_0$. For large S, usually encountered for O^- bound polarons, their envelope is proportional to

$$\exp(-w(\hbar\omega - 4E_{\mathrm{P}})^2) \qquad \text{with } w^{-1} = 8E_{\mathrm{P}}\hbar\omega_0. \tag{10}$$

The absorption band $\alpha(\hbar\omega)$ for a two-well transition thus is given by

$$\alpha(\hbar\omega) \propto (J^2d^2/\hbar\omega) * \exp(-w(\hbar\omega - 4E_{\mathrm{P}})^2). \tag{11}$$

Equation (11) indicates that both a high oscillator strength and the largest possible ratio width/peak energy, which can occur for a homogeneous absorption band, are characteristic for small polaron absorptions. The cause of the high oscillator strength is, beside the occurrence of an electric dipole allowed charge transfer transition, the large transition dipole length d, weighted by $J/\hbar\omega$ (equation (8)). The ratio of half-width at half-maximum (HWHM), W, to peak energy, M, is

$$W/M = \sqrt{2\ln(2)S(\hbar\omega_0)^2}/S\hbar\omega_0 = \sqrt{2\ln 2/S} \tag{12}$$

whereas for a typical colour centre, where an additional electronic excitation, E_{el}, occurs, this ratio is smaller, $\sqrt{2\ln(2)S(\hbar\omega_0)^2}/(S\hbar\omega_0 + E_{\mathrm{el}})^2$, assuming the same S and $\hbar\omega_0$. Alternatively, the quantity W^2/M can be considered as a fingerprint for small polaron absorption:

$$W^2/M = 2\ln(2)\hbar\omega_0. \tag{13}$$

which is independent of S. It thus provides a general test for small polaron optical bands, irrespective of their peak energies. The value of W^2/M is expected to be close to 0.14 eV, obtained for an estimated typical LO phonon energy of 0.1 eV. In comparison, for a typical colour centre, the F centre in KBr at 20 K [22], W^2/M is much smaller experimentally, about 3 meV. It should be noted that the given estimate of W^2/M is valid for an optical charge transfer of a carrier between any equivalent ions of an oxide material, not necessarily oxygen ones. A W^2/M value close to 0.14 eV, however, becomes a strong indication for bound O^- polaron bands if the presence of holes at equivalent oxygen sites is proved, and in the absence of charge carriers able to be localized at other equivalent ions. Bound holes furthermore are characterized by large polaron stabilization energies in oxide materials, often near 1 eV, leading to band peaks in the visible or near infrared. For further details see below.

The band predicted by equation (11) for bound polaron absorption is essentially symmetric with respect to the peak energy $4E_{\mathrm{P}}$, for the present two-well case. We mention here that absorptions of real bound polaron systems already tend to be asymmetric, with the high energy side raised above the expectation expressed by equation (11). There are indications, see further arguments below, that this is caused by transitions to final states having energies higher than the equivalent ones; only the latter type were taken into account when deriving equation (11). It is merely the low energy onset of the absorption which is caused by transitions between equivalent initial and final states.

The temperature dependence of the bandwidth is described by the substitution [23] $w^{-1}(T) = w^{-1}(0)\mathrm{Coth}(\hbar\omega_0/2kT)$ in equation (10), leading to $w^{-1}(T) = \sqrt{16E_{\mathrm{P}}kT}$, if the thermal excursions of the configurational coordinate at the initial state dominate the zero-point excursions. Experimentally, it is found, e.g., that the width of a typical O^- bound polaron absorption in MgO:V^- increases by 3% between 5 and 295 K [24]. For small polarons another type of temperature dependence can occur, because on account of the equivalence of initial and final states there are also low lying final states which can be populated at rather low temperatures. Emission from such states to the ground state contributes a term proportional to $-\exp(-\hbar\omega/kT)$ to the total optical spectrum [1, 3, 4, 25]. For high coupling strengths S, typical for O^- bound polarons, however, the transition probabilities for low energy stimulated emissions are equally weak as for the corresponding absorptions—see equation (9); therefore, such terms can be neglected for the present systems.

It is seen that optical absorption of small polarons (equation (11)) is a convenient means for directly determining the stabilization energy, E_{P}, at one site through lattice distortion. This contribution is, however, only one part of the total energy of the charge carrier, E_{tot}; it is further determined by the increase of the kinetic energy, E_{kin}, of the hole, when localized. The size of the latter can only be estimated or calculated by more elaborate quantum chemical methods, in

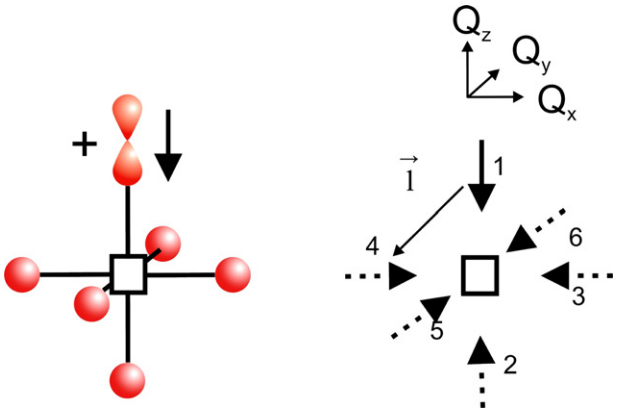

Figure 4. Left: model of a Mg vacancy in MgO, next to which a hole (+) has been trapped, accommodated in a σ-type 2p orbital of O^- (a possible s–p hybridization has not been taken into account). Right: the orbital, assumed to be occupied initially by a hole, is symbolized by a full arrow at 1. The equivalent, initially unoccupied ones at sites 2 to 6 are shown dashed. The coordinate system at the top indicates the three components of a T_{1u} (O_h) symmetry lowering vibration of the octahedral complex. One of the four possible paths for light induced charge transfer between neighbouring orbitals is indicated by a thin arrow ($1 \rightarrow 4$), symbolizing a transition vector $\vec{l}$.

contrast to the determination of E_P. For a free, uncoupled charge carrier it is usually assumed that E_{kin} is raised by half the width of the band in which it moves in order to localize it at one unit cell. A carrier localized in this way will thus have a level at the edge of the corresponding band, and polaron formation would then shift the level from the edge into the band by the polaron energy E_P. For oxide crystals E_P is generally not sufficient for overcompensating E_{kin} and ideal free small hole polarons are not known to our knowledge. The situation is different for a hole in the field of an attracting acceptor. Here the kinetic energy of the localization near the defect tends to be partly or totally compensated by the Coulomb attraction. The polaron formation at one of the equivalent oxygen neighbours next to the acceptor then again has to compete with the corresponding rise of E_{kin}, but this is usually outweighed by lattice distortion (for further details see section 4). The level energy of the acceptor usually turns out to be of the order of E_P.

Optical excitation of a hole from such a level, for the two-well case occurring with the highest probability for photons with energy $4E_P$ (equation (11)), will then lead to final states resonant with the valence band. It is thus not astonishing that in most realized cases the optical absorption of bound small polarons will quench itself. The coincidence of the polaron excited states with the delocalized Bloch levels facilitates the diffusion of the hole away from its localizing acceptor.

3.2. Six-well system

Next in simplicity to the introducing two-well situation is the case of a polaron potentially forming at one of six equivalent O^{2-} sites. This situation is realized, e.g., for a hole trapped at one of the O^{2-} ions next to the Mg vacancy in MgO, labelled MgO:V^-. As deduced from the EPR analysis, the hole is in a 2p orbital at one oxygen site, having an axial σ-type orientation with respect to the vacancy, as sketched in figure 4.

The transfer between the corresponding hole positions and the coupling to the lattice is given by a Hamiltonian, which has a structure that is a straightforward generalization of

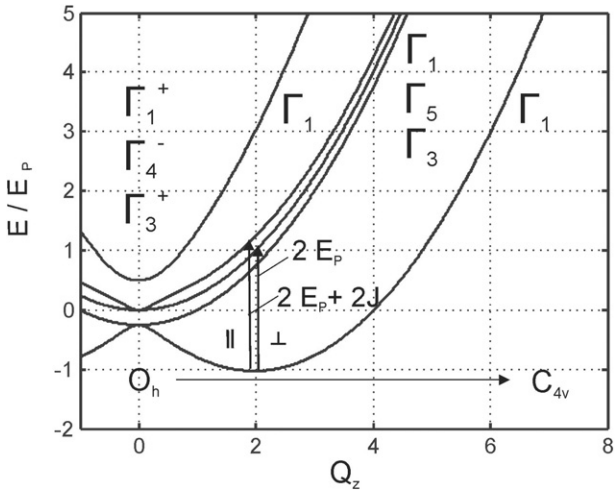

Figure 5. The eigenvalues of an octahedral six-well system, equation (13), depending on a Q_z-type tetragonal distortion, lowering the symmetry from O_h to C_{4v}. The values $J = (1/2)\hbar\omega_0$ and $E_p = 4\hbar\omega_0$ have been assumed for visualization. Only the transitions indicated by the vertical arrows are electric dipole allowed.

that pertaining to the two-well situation (equation (3)). It mirrors the topology of the present system:

$$H = \begin{pmatrix} VQ_z + S & 0 & J & J & J & J \\ 0 & -VQ_z + S & J & J & J & J \\ J & J & VQ_x + S & 0 & J & J \\ J & J & 0 & -VQ_x + S & J & J \\ J & J & J & J & VQ_y + S & 0 \\ J & J & J & J & 0 & -VQ_y + S \end{pmatrix}$$

$$\text{operating on} \begin{pmatrix} 1 \\ 2 \\ 3 \\ 4 \\ 5 \\ 6 \end{pmatrix}. \tag{14}$$

Its eigenvalues for the static case, depending on one of the three degenerate tetragonally distorting coordinates, Q_z, are given in figure 5. On the basis of the symmetries involved in the problem—O_h in the undistorted case which is lowered to C_{4v} by distortion—an overview on the symmetries and degeneracies of the expected eigenstates can be found from group theory [26]. Here we prefer to give an explanation of the features occurring with more direct physical arguments. The splittings into states transforming as Γ_3, Γ_5 and Γ_1, related to the distorted C_{4v} symmetry, result from the transfer between the equivalent equatorial sites 3, 4, 5 and 6 (figure 5), which remain equivalent after optical excitation. It is borne out by experiment, see below, that the transfer of a hole between these sites occurs so fast that the lattice does not relax to a new equivalent polaron ground state before such a transfer to a neighbouring site. Therefore molecular orbitals form, transforming according to the given representations, and the predicted polarizations of the absorption bands are observed.

This is seen in the optical absorption spectrum of this defect, observed at 5 K (figure 6). A wide band is found, peaked near 2.3 eV, which has two components, polarized parallel and

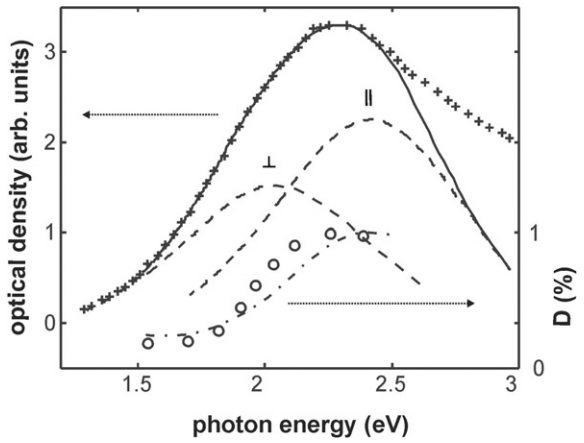

Figure 6. Optical absorption of MgO:V^- and of its electric field induced dichroism ($D = (I_\perp(E) - I_\parallel(E))/I_\perp(0)$) with transmitted intensities I_i [27]. The full, dashed and dash–dotted lines indicate the simultaneous fits of both data sets using equation (15) and the parameters in table 1. Note that the total absorption band is based on an equal-probability distribution over all three orientations, whereas the dichroism results from alignment into only one direction. This explains why the zero of the dichroism does not coincide with the crossing of the parallel/perpendicular absorption bands [26].

perpendicular to the distortion direction. Rose and Cowan [27] and Henderson [28] found definite evidence for the existence of these two components by aligning the C_{4v} defect axes using an electric field. The dichroism ($(I_\perp(E) - I_\parallel(E))/I(0)$, I transmitted intensities), measured under this condition, is also shown in figure 6.

Since the total absorption of such a six-well system can be assumed to result from the superposition of four two-well transitions as treated above—one of such transitions is symbolized by the narrow arrow between sites 1 and 4 in figure 4—the absorption bands are expected to have the same shapes:

$$\alpha_\parallel \propto (|\vec{l}|_\parallel/\omega) * \exp(-w(\hbar\omega - 2E_\mathrm{p} - 2J)^2) \qquad \text{with } w^{-1} = 4E_\mathrm{p}\hbar\omega_0 \quad (15a)$$

$$\alpha_\perp \propto (|\vec{l}|_\perp/\omega) * \exp(-w(\hbar\omega - 2E_\mathrm{p})^2) \quad (15b)$$

where the prefactors denote the projections of the transition vectors on the centre axis and perpendicular to it, respectively. It should be noted that $\vec{l}$ may not point exactly along 45° with respect to the axis of the defect because the ideal geometry of the defect is distorted by hole capture [26].

A simultaneous fit of these relations to the total absorption and the dichroism is represented by the full, dashed and dash–dotted lines in figure 6. The following parameters led to a reasonable reproduction of the experimental data: $E_\mathrm{p} = 1.08$ eV, $J = 0.18$ eV, $\hbar\omega_0 = 0.06$ eV.

It is seen that the optical absorption features typical for MgO:V^- are well reproduced by the polaron model. Competing explanations, to be discussed below in section 4, were not able to account for the observations adequately. Also the high oscillator strength of V^-, ~0.1 [29], is in accord with the polaron model.

We mention a few further experimentally established facts about V^-, which are in line with the accepted model of MgO:V^- and the present interpretation of its optical absorption. The tunnelling between the ground states of the polaron at each of the equivalent six wells has been found [30] to be $J_\mathrm{gg} = 0.8 \times 10^{-7}$ eV. Such zero-phonon (diagonal) processes ($n = 0$ in equation (9)) are reduced by the factor e^{-S}, with the Huang–Rhys factor $S = 2E_\mathrm{p}/\hbar\omega_0$

Table 1. Parameters used to describe the small polaron optical absorption of various O^--type centres in the alkaline earth oxides [26].

Centre	Band peak (eV)	J (eV)	E_p (eV)	$\hbar\omega_0$ (eV)
MgO:V^-	2.30	0.18	1.08	0.06
MgO:Na	1.58	0.18	0.67	0.05
CaO:V^-	1.85	0.24	0.72	0.08
CaO:Li	1.74	0.28	0.66	0.08
CaO:Na	1.39	0.23	0.57	0.06

in the present six-well case; we thus predict $J_{gg} = J * e^{-S} = 0.6 \times 10^{-7}$ eV on the basis of the optically determined values for J and E_p (table 1). Also the optically detected magnetic resonance (ODMR) of MgO:V^-, measured via the changes of the magnetic circular dichroism (MCD) under conditions of paramagnetic resonance, has recently been found to be fully consistent with the predictions of the polaron model [31]. These results, to be published separately, especially show that the variations of the ODMR with the direction of $\boldsymbol{B}$ are in accord with the established localization of the hole at one oxygen site, in contrast to an earlier report by Izen *et al* [16]. Whereas the polaron absorptions treated here relate to the optical transitions between the ground state orbitals at each well, studies of the MCD also allow one to identify transitions to higher lying states, e.g. crystal field final excited states. These features can be based on an extension of the present polaron model and will be reported in another publication. Here we concentrate solely on the phenomena arising from the orbital ground states at each well, leading to the onset of the small polaron based optical absorptions at the lowest energies. Because of the already mentioned additional transitions to higher lying states at the final sites, the observed total O^- related absorption bands are usually asymmetric, with raised intensity at higher energies.

As an aside, we point out that the present sample case, V^-_{Mg} in MgO, is the antimorph of V^+_O, usually called an F^+ centre. In the latter case one electron is captured at an oxygen vacancy, and the cubic symmetry is unbroken. The V^-_{Mg} centres, on the other hand, like all the other bound small polaron systems, offer an excellent example for broken symmetry.

Further variants of MgO:V^- include those where in addition Al^{3+}_{Mg} is associated at the next nearest cation site, or OH^- or F^o at the nearest anion positions beyond the Mg vacancy, as seen from the O^- position [33]. The associated centres tend to have absorption maxima shifted by about 0.1 eV towards lower energies [33].

Several additional O^- defects in MgO and other alkaline earth oxides are known which all follow the six-well scheme, around which the present subsection is centred. A detailed list of such centres and their EPR parameters has been compiled by Henderson and Wertz [32]. Table 1 contains those among them where the optical absorption has been interpreted on the basis of the small polaron model. As a general rule it is found that the polaron stabilization energy decreases if the effective charge of the binding acceptor is lowered or if the lattice constant increases [34].

All of these defects can be aligned under an electric field or uniaxial stress [27, 28], unless they are locked by associated compensating ions. Freely orientable axes of V^- centres align parallel to the electric field and to the stress axis [27]. This has been modelled theoretically [6, 34], although it appears to be in conflict with the finding, based on EPR studies, that the acceptor—O^- distances are typically larger by 30–40% than the corresponding lengths in ideal crystals. Apparently the entire distortion field, not only the one lengthened distance, determines the stress response.

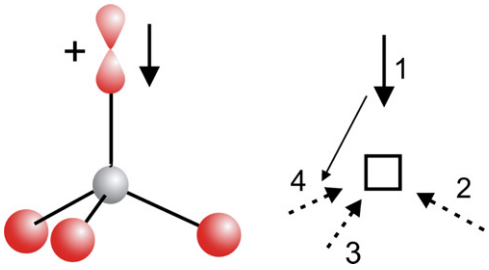

Figure 7. Model of an O^- polaron bound to an acceptor in tetrahedral symmetry. Symbols with the same meanings as in figure 4 are displayed.

It should be added that the O^- polaron in MgO:Li, which can be prepared stably by chemical means [35], acts as a defect catalysing the deprotonation of methane, if present at the surface of MgO (see e.g. Catlow *et al* [36]).

3.3. Four-well system

Also the capture of a hole at one of four O^{2-} ions, next to an acceptor defect in tetrahedral symmetry, can lead to the formation of a bound O^- polaron. Figure 7 shows such a situation.

In analogy to the previous cases, the corresponding Hamiltonian is

$$H = \begin{pmatrix} VQ_{xyz}+S & J & J & J \\ J & VQ_{\bar{x}y\bar{z}}+S & J & J \\ J & J & VQ_{\bar{x}\bar{y}z}+S & J \\ J & J & J & VQ_{x\bar{y}\bar{z}}+S \end{pmatrix} \text{ operating on } \begin{pmatrix} 1 \\ 2 \\ 3 \\ 4 \end{pmatrix} \tag{16}$$

with $Q_{\bar{x}y\bar{z}} = -Q_x + Q_y - Q_z$ etc, where the Q_i are orthogonal [100]-type configuration coordinates of the tetrahedron.

Its eigenvalues, depending on Q_{xyz}, which describes a distortion having the symmetry of one of the trigonal axes, are shown in figure 8. In this case the transition energy at fixed Q is $(8/3)E_P$, except for the additional tunnelling shifts [37]. The corresponding absorption bands thus are expected to be described by

$$\alpha_{\parallel} \propto (|\vec{l}|_{\parallel}/\omega) * \exp(-w(\hbar\omega - 8/3E_p - 2J)^2) \tag{17a}$$

$$\alpha_{\perp} \propto (|\vec{l}|_{\perp}/\omega) * \exp(-w(\hbar\omega - 8/3E_p + J)^2) \tag{17b}$$

with

$$w^{-1} = (16/3)E_p\hbar\omega_0.$$

As an example the optical absorption of BeO:Li is presented [37]. In this system, an O^- hole, produced by x-irradiation, is captured at one of the four oxygen ligands of the Li_{Be} acceptor [38]. BeO crystallizes in the wurtzite structure, characterized by a polar axis c, and thus the four oxygen ions are not quite equivalent. It turns out that a hole at the axial site is more stable by 34 meV [38]. Since this implies that there is practically exclusive alignment of the hole along the c-axis at low temperatures, it is straightforward to identify both absorption components (equation (17)). Figure 9 shows that light polarized parallel to the c-axis, and thus also parallel to the distortion axis, is absorbed with a band peaked near 2.6 eV, which can be reproduced by equation (17*a*), using the parameters $E_P = 1.18$ eV and $\hbar\omega_0 = 0.10$ eV. The ratio $W^2/M = 0.17$ eV is typical for bound small polaron absorption.

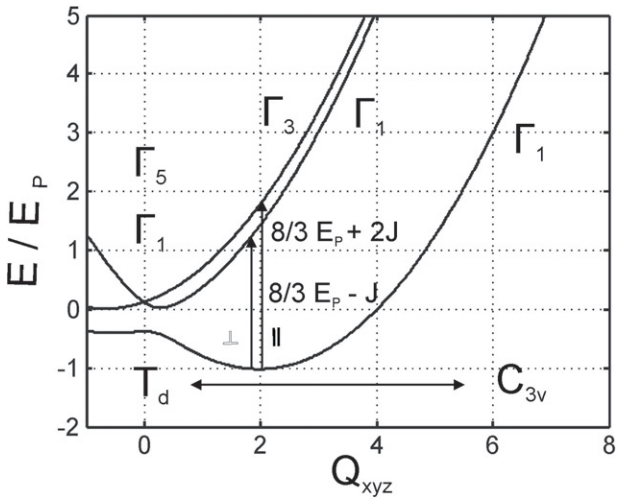

Figure 8. The eigenvalues of a tetrahedral four-well system, equation (16), depending on a distortion coordinate along one of the trigonal axes.

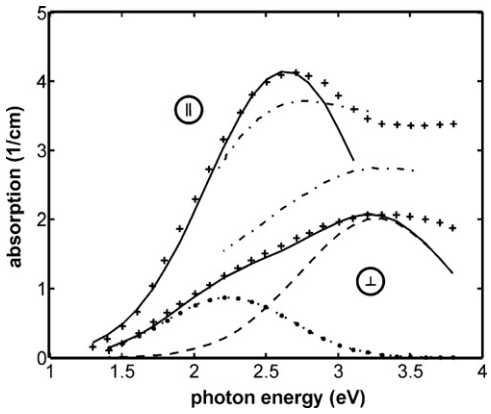

Figure 9. Optical absorption of BeO:Li [37, 39]. Lower part: polarization perpendicular to the centre axis; upper part: polarization parallel to the centre axis. The dash–dotted lines correspond to polarized absorptions at room temperature; all other experimental data (+) were taken at 6 K. The full lines represent interpretations based on the crystal field plus small polaron transitions (lower part) and small polaron transitions only (upper part). For further details see the text.

For $\vec{E} \perp c$, the peak of the band is near 3.2 eV. According to equation (17*b*), predicting a shift from the peak of the parallel band (equation (17*a*)) by $3J$ (figure 8), this corresponds to $J = 0.2$. Equation (17*b*) can now be used to predict the polaron absorption for perpendicular absorption, using the parameters determined from the parallel band. However, if only this contribution (equation (17*b*)) is considered, there is a discrepancy between prediction and experiment at low energies for perpendicular polarization. This difference can be attributed [39] to a $2p_z \rightarrow 2p_x$, $2p_y$ crystal field transition, as supported by the following arguments. (1) By symmetry this transition occurs only for perpendicular polarization, as observed. (2) It is weaker than the typical polaron transition (equation (17*b*)), although the short bond length of BeO, 0.165 nm, favours s–p hybridization and thus a higher intensity than for MgO:V^- (bond length 0.210 nm). (3) The peak energy of the additional band, 2.1 eV, is compatible with the

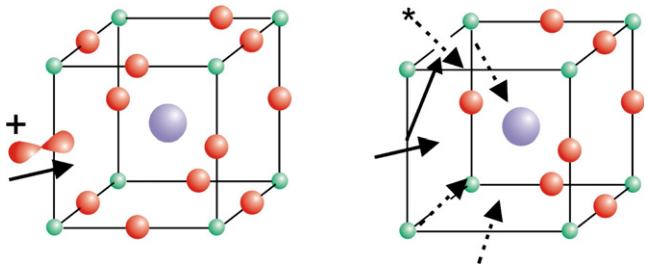

Figure 10. An O^- hole bound to an acceptor on an A site in an ABO_3 oxide perovskite (e.g. Na^+_{Ba} in $BaTiO_3$). Left: a hole captured at one of the twelve equivalent O^{2-} ions next to the acceptor is indicated. Right: symbols as in figure 4. Only the equivalent oxygen ions next to the initial site are shown by dashed arrows. A light induced charge transfer to one representative neighbour (*) is indicated.

crystal field splitting derived from $\Delta g_\perp = 0.0184$ for BeO:Li [38]. See section 4 for further details.

With temperature rising from 5 to 295 K, the maxima of the absorption intensities shift towards each other, reflecting the increasing population of the energetically less favourable non-axial hole positions.

3.4. Twelve equivalent neighbours

An acceptor ion on an A site in an ABO_3 oxide perovskite is surrounded by twelve equivalent O^{2-} ions, and a hole can be captured at each of them with the same probability. An example of such a defect is a Na^+ ion replacing Ba^{2+} in $BaTiO_3$ [40]. The slight trigonal distortion of the material in its low temperature rhombohedral phase is neglected. An optical absorption by bound hole polaron transfer is expected to occur as indicated in figure 10. Because the hole will be transferred with the highest probability only to its first equivalent neighbour orbitals, only these four are shown, together with one of the possible transfer directions, connecting the initial orbital with one representative neighbour, labelled by an asterisk (*). The expected optical absorption shape is deduced qualitatively from the previous treatments. Again a Gaussian-type band will occur, but this time peaked at about $1E_p$, as discussed in the next subsection. A splitting caused by tunnelling among the final states has not been identified so far and is thus not taken into account.

Experimentally the optical absorption of this system was monitored by measuring its light induced change (figure 11), simultaneously with the corresponding EPR signal of the trapped hole [40]. The band is peaked near 1.4 eV, an energy much lower than in the previous cases. A natural explanation is given in the next subsection. As discussed there, it is predicted that the absorption for the twelve-site case is given by

$$\alpha(\hbar\omega) \propto 1/\hbar\omega * \exp(-w(\hbar\omega - E_P)^2) \qquad \text{with } w^{-1} = 2E_P\hbar\omega_0. \tag{18}$$

The parameters leading to the best fit (figure 11) are $E_p = 1.4$ eV, $\hbar\omega_0 = 0.08$ eV and $W^2/M = 0.12$ eV.

3.5. The dependence of absorption peak energies on topology

Experimental evidence was presented above that the absorption peak energies decrease if the number of equivalent oxygen positions neighbouring an acceptor increases from two to four, six and twelve. Here we want to point out the physical reason for this phenomenon.

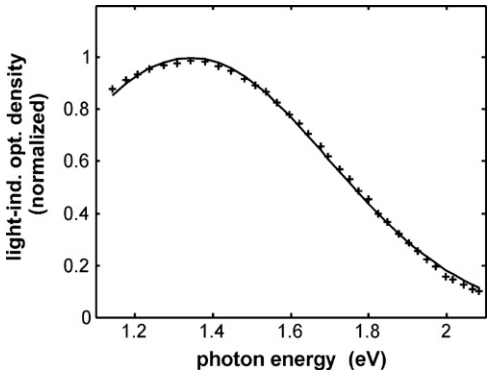

Figure 11. Light induced optical density caused by O^- next to Na in $BaTiO_3$:Na [40] as interpreted using equation (17) with the parameters $E_P = 1.4$ eV, $\hbar\omega_0 = 0.08$ eV ($W^2/M = 0.12$ eV). The energy range shown was limited by the spectrometer used for monitoring EPR changes simultaneously with the absorption changes.

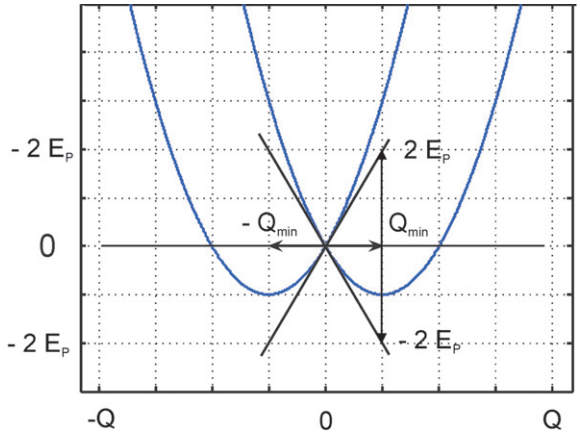

Figure 12. The total static energies of a two-well system, resulting from the addition of the elastic energy of the vibration to the change of the hole energies under distortion. These hole energies, $\pm V\,Q$, are also shown separately by the straight lines.

We start by illustrating the total energies of a two-well system (figure 12), comprising the sum of the electronic (hole) and lattice energies. Only the hole part interacts with light (in the spectral range of interest), whereas it is the passive role of the lattice to follow the transferred hole. It is most straightforward, therefore, to base the intended argument on the hole energies, $\pm V\,Q$, shown by straight lines in the graph. If the system is stabilized at the right well with a polaron energy E_P, the hole energy has decreased to $-2E_P$. Under interaction with light the hole is transferred, with the lattice assumed to be fixed at Q_{min}, to the corresponding hole potential of the left well, having energy $+2E_P$ at Q_{min}. Thus the complete hole energy change under absorption is $4E_P$. This explains why the polaron absorption of a two-well system is peaked at $4E_P$.

The argument can be generalized to the other topologies, if one realizes that the energy of the final position is biased by the stabilization at the initial one. The increase of the hole energy

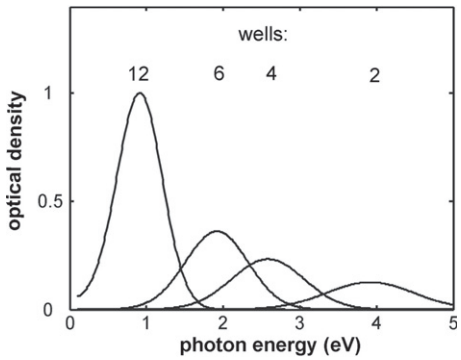

Figure 13. Dependence of relative optical densities on the number of equivalent oxygen sites. For twelve wells the absorption band has been normalized to 1. Parameters used: $E_P = 1$ eV, $\hbar\omega_0 = 0.08$ eV. This leads to $W^2/M = 0.11$ eV for all well numbers, independent of the various peak positions, alias the corresponding different Huang–Rhys factors.

at the final position at Q_{min} by $2E_P$ for the two-well case is caused by this bias. Apparently, it is the projection of the final distortion on the initial one which counts (see figure 12). For the two-well system the angle between initial and final distortions, Q_{min} and $-Q_{min}$, is 180°; therefore the projection is proportional to the corresponding cosine, -1. The minus sign indicates that the final hole energy lies above the initial one; figure 12.

The situation of six equivalent sites is almost as simple. Here the distortion at the final site, one of the equatorial positions in figure 4, is perpendicular to that of the initial one; therefore the projection of the final distortion on the initial one is zero and thus the peak energy of absorption is $2E_P$, the amount of the hole energy at the initial site. Here the lowest quanta absorbed have enough energy to lift the hole out of its initial well ('to strip it from its phonon cloud'), where the hole energy is $2E_P$. For a system with four equivalent sites, having tetrahedral symmetry, the projection of the initial distortion on the final one is $-1/3$; accordingly the absorption is peaked at $2E_P + (2/3)E_P = (8/3)E_P$. This argument can be generalized to the case of twelve oxygen ions neighbouring an acceptor. By symmetry, here the distortion direction from one O^- ion to the central acceptor points along a $\langle 110\rangle$-type direction; see figure 10. The cosine between distortions at neighbouring sites thus is $+1/2$, where the plus sign indicates that the energy of excitation from initial to final state is less than $2E_P$. In fact it is only $1E_P$, since initial and final distortions have some parallel components. On this basis the peak energy for the twelve-well arrangement in equation (17) was taken as $1E_P$. Figure 13 visualizes the dependence of the optical densities on oxygen coordination number. The lower coordination numbers lead to lower peak intensities, because of both their larger widths and the prefactor $1/\omega$. It can be added that the peak energies for the—so far fictitious—clusters of three and eight equivalent oxygen ions are $3E_p$ and $(4/3)E_p$, respectively.

For this argument, resulting in figure 13, a constant E_P has been assumed. Of course, depending on the charge of the acceptor, the lattice constant or the extent of the hole orbital, E_P will surely change, as seen e.g. in table 1. Therefore the actual band peak is determined not only by the topology but also by the E_P valid for the given defect.

Excited state splittings, caused by resonance transfer among the final states, have not been considered in figure 13. It should be noticed that in the two-well case there is no such splitting, because there is only one single excited state. For all the other symmetries there are equivalent excited states, allowing corresponding resonance splittings. They have been resolved for six and four wells (figures 6 and 9, respectively). It turns out, furthermore, that the signs of

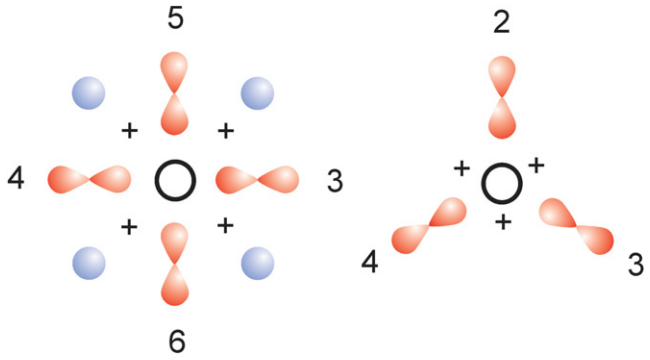

Figure 14. With reference to the sign of J in the octahedral (left) and the tetrahedral (right) situations. The acceptor positions are marked by the open circles. The excited tunnelling states are expected to be combined by the excited state oxygen hole orbitals shown, labelled by the same numbers as in figures 4 and 7. The sign of J is determined by the sign of the potential prevailing in the regions of strongest overlap, estimated to be near the points marked (+). In the octahedral case hole density would be repelled there by the influence of the positive nearby cation (e.g. Mg^{2+}) and by the oxygen cores. Therefore tunnelling hole states having nodes are favoured energetically in the octahedral situation. In the tetrahedral case hole repelling cations (not shown) are further away and the hole attracting acceptor potential is near the region of highest hole overlap density. Therefore the node-free hole tunnelling state is stabilized.

J are different for the two cases. As deduced by continuity from the polarized absorptions, determined for the distorted geometries (figures 6 and 9), by extrapolating to the undistorted situations, one finds that for the octahedral case O_h the Γ_3^+ hole state, having nodes, would be the ground state, whereas for the tetrahedral T_d situation the node-free Γ_1 hole state would be lowest. The latter sequence appears to be universal for tetrahedral symmetry; it has also been found for Se^- next to the Zn vacancy in ZnSe [41]. Interpreted in physical terms, this means that for the four-well situation, holes are attracted to the regions between the oxygen ions, determining the sign of J, whereas they are repelled for the six-well situation [26]. Qualitatively, this can be understood on the basis of figure 14. It appears to be caused by the fact that in the tetrahedral situation the orbitals have their strongest overlap near the site of the hole attracting negative acceptor, whereas for the other case they tend to have stronger overlap between the oxygen ions, being repelled by both cores and by a positive cation nearby (figure 14).

In passing one can ask whether for free small polarons a biasing of the final site by the distortion of the initial one can also be expected. In such cases it is generally assumed that a carrier is transferred from its initial well, where the electronic energy is $-2E_P$ to a completely undistorted, i.e. unbiased, final site. Under this premise the corresponding absorption of free polarons is thus predicted to be peaked near $2E_P$. It is, however, quite unlikely that the final site is not influenced by the distortion of the initial one. Charge transfer transitions are strongest between neighbouring equivalent sites, as indicated by the arrows in figure 15. The ion common to adjacent octahedra is distorted into opposite directions for the initial and final situations. Therefore for free polarons also there is a slight bias of the final state by the initial one. Thus a polaron energy E_P deduced from the absorption band of free polarons on the basis of the conventional theory is rather an upper bound to the real one.

In spite of the fact that there is only a slight bias of the final level by the polaron localization at the initial site for free small polarons, their optical absorption is sometimes discussed using a scheme like that of a two-well bound polaron, as in figure 3, apparently implying that the final level, in contrast, is strongly biased by the occupation of the initial position. Mott

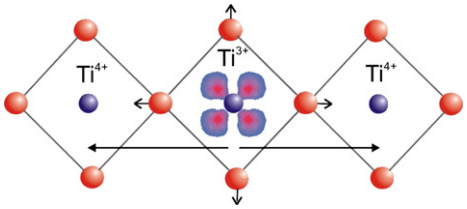

Figure 15. Model for a typical light induced small polaron transfer for a conduction electron in $BaTiO_3$, as an example. Initially, the electron has d_{xy} character at a Ti site, repelling its O^{2-} neighbours as indicated. After light induced transfer to neighbouring sites, as modelled by either of the two arrows, the O^{2-} ion common to both initial and final sites is not adapted to the presence of the electron at the final site. Its initial distortion thus biases the energy at the final site.

and Austin [42] have shown that this is an artefact. It is only by using a transformation of the configuration coordinates used that the case of, essentially unbiased, free small polaron absorption can be mapped on a graph like figure 3. The physics is not changed, of course, by this transformation and the absorption peak for free polarons is still predicted to be near $2E_P$.

4. Interpolaron or intrapolaron transitions?

As stated in section 2, the orbital energy levels of O^- ions, threefold degenerate in cubic symmetry, are split into up to three crystal field states in the actual local surroundings (figure 1). It is thus not surprising that initially the optical absorptions of O^- defects were attributed to transitions between such levels [43]. This approach was exposed to a stringent test when rather complete experimental data on the structure and optical absorption of the model system MgO:V^- became available. In section 3.3 it is reported that its oscillator strength f is rather large, ∼0.1. An assignment to p–p-type crystal field transitions, being Laporte forbidden, thus became doubtful, even if some s–p hybridization, expected at the not inversion symmetric O^- sites, was taken into account. As a further discrepancy the level separations, determined by evaluation of the g-tensor elements (equation (1)) on the basis of the O^- spin–orbit coupling ($\lambda \sim 135\ cm^{-1}$) [43], led to values around 1.5 eV instead of the peak position near 2.3 eV, observed for MgO:V^-. For a complete overview on such discrepancies, see [32].

In section 3.4 (figure 9) a case was shown, BeO:Li, where the optical absorption points to the appearance of an O^- crystal field transition [39]. As discussed, the comparatively short bond length of BeO leads one to expect a sizable s–p hybridization and a corresponding increase of the transition intensity. Still, even in this case, the corresponding intensity (figure 9) is weaker than that of the accompanying competing transitions.

A new approach to the explanation of the O^- absorption bands of MgO:V^-, avoiding the difficulties of the crystal field model, was proposed in 1974 by Schirmer *et al* [24]. They introduced what can now be called 'interpolaron' charge transfer transitions. The arguments presented in the previous sections of the present review result from the model put forward in this early publication. In order to derive the properties of the absorption bands, the authors initially set out to calculate the moments of the absorption bands. Two years later the treatment was recast into the general language of colour centre physics [26], i.e. along the lines used in this article. As demonstrated above, this model, introducing interpolaron charge transfer transitions rather than the previously invoked intrapolaron crystal field excitations, correctly predicts the main features of the O^- defects: high oscillator strengths, wide bands, peak positions not correlated with the energy splittings derived from g-tensors, excited state resonance splittings, electric and stress alignment of the defects, dielectric and anelastic relaxations.

In 1977 Norgett *et al* [6] substantiated this phenomenological polaron model through a detailed calculation of the essential parameters occurring in this approach, using quantum chemical and shell model methods. First they addressed the question of why there is localization of the hole at only one site, although its kinetic energy can be lowered considerably if it is delocalized over all six oxygen neighbours of the vacancy. The energy decrease by lattice polarization of a localized hole outweighs this contribution, as turns out from the calculations. The physical basis [44] for this result is the fact that the lattice distortion depends on the square of the local charge density. For a hole delocalized on the six oxygen neighbours of V_{Mg} in MgO the charge at each site is 1/6 of the total one, being present at one site in the case of complete localization. Comparing the two situations, it is shown that the resulting energy lowering by localization at one site is increased by a factor of 6 compared to that for the case of delocalization. This source of stabilization can thus have a stronger influence than kinetic energy lowerings by delocalization. Second, these authors [6] approximately reproduced the observed peak energy, ∼2.3 eV, by calculating the optical transition energy under fixed ionic positions, i.e. under Franck–Condon conditions. Three considerations were essential to arrive at this result:

(1) All electronic polarizations of the system immediately follow the hole, transferred from its initial O^- site to a neighbouring O^{2-} ion, in a fixed ionic framework. This contribution thus is absent in models not allowing for electronic polarization at the ions involved.
(2) It had to be considered that the crystal field splitting of the O^- orbitals, after optical transfer of the hole to the new site with the ion positions kept fixed, differed from that in the initial, ionically relaxed situation.
(3) The lowering of the optical levels by excited state tunnelling (see section 3.3) was included semiempirically.

On this basis also further intrinsic properties of MgO:V^- were modelled successfully: the electric and elastic dipoles formed by the association of an O^- ion with the acceptor, here V^-, as well as the hole ionization energy of the V^- acceptor. The latter was predicted to be 1.6±0.2 eV in good agreement with the experimental value. In 1979 Harding [34] demonstrated that also the corresponding O^- bound polaron features of the other alkaline earth oxides, CaO and SrO, can be treated along the same lines.

5. Bound O^- polaron optical absorption in further materials

5.1. General remarks

The polaron systems treated so far contain essentially equivalent oxygen sites. But also arrangements with inequivalent positions, present in material structures of lower symmetry, can exhibit similar optical phenomena, and there is a continuous transition to such systems. In all cases the underlying absorption mechanism is charge transfer between O^- and O^{2-}. Inequivalence of such sites leads to the following modifications: a hole now is locked more deeply at one of the sites and, as indicated in figure 16, there is an increase of the optical excitation energy by E_{el}, the hole energy difference between initial and final sites in the respective equilibrium situations. Furthermore, according to equation (7), the transition intensity will decrease, because the mixing between initial and final states (equation (7)) will be attenuated by the increasing energy difference between the equilibrium states of equivalent and inequivalent sites. The sample systems presented in the following subsections will include some with equivalent sites along with a few having inequivalent initial and final positions.

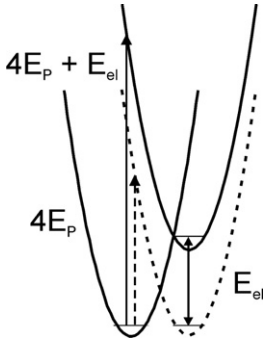

Figure 16. Final state potential energy sheets for equivalent (dashed) and inequivalent initial and final sites in a two-well cluster.

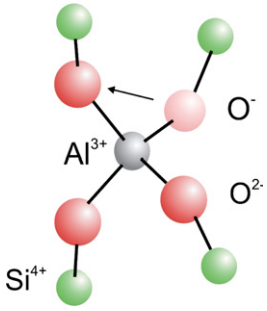

Figure 17. Section of quartz crystal (as viewed along its c-axis) around an Al^{3+} (or Ge^{4+}) defect on a Si^{4+} site. A hole has been captured at one of the neighbouring O^{2-} ions. Among the possible charge transfer paths, one is symbolized by a thin arrow.

5.2. Systems with essentially tetrahedral symmetry

5.2.1. Quartz. In crystalline quartz (here and in the following: α-quartz) two O^--type defects are known, O^- next to Al^{3+}_{Si} [45] or to Ge^{4+}_{Si} [46], which show absorption bands typical for bound hole polarons; figure 17. Al^{3+} is charged negatively with respect to the replaced Si^{4+} and can thus stabilize a hole at a neighbouring oxygen ion by Coulomb attraction. Germanium is amphoteric in quartz, i.e. Ge^{4+} can trap an electron as well as a hole [46]. In the two cases the electronic structures of the O^- defects are similar: the ground state 2p lobe is oriented perpendicular to the plane spanned by Al(Ge), O^- and Si^{4+}; see figure 17. This non-bonding π-orientation is favourable for the hole because of the lack of near bonding partners and the relatively high charge of Si^{4+}, repelling the hole (see the remark in section 2.2) in a σ-configuration. Since the Al(Ge)–O^-–Si ions are arranged in an almost straight line, the energies of the two lowest orbital states are quite close to each other, like in figure 1(b), and the largest Δg values are measured for $\boldsymbol{B}$ approximately parallel to (Al(Ge)–O^-) [47].

Among the three bands, A_1, A_2 and A_3 (figure 18), usually observed in smoky quartz, only A_1 and A_3 are correlated with the EPR of the ground state of the already mentioned SiO_2:Al EPR centre. This was demonstrated by ODMR studies of the defect [50]. The relatively high peak energy of A_3, $M = 2.85$ eV, is consistent with O^- in a tetrahedral arrangement; see section 3.4. From this energy, predicted to be $(8/3)E_p$ for this situation (section 3.4), we estimate $E_p \sim 1.07$ eV, close to the value found for BeO:Li, 1.18 eV [37]. Also the

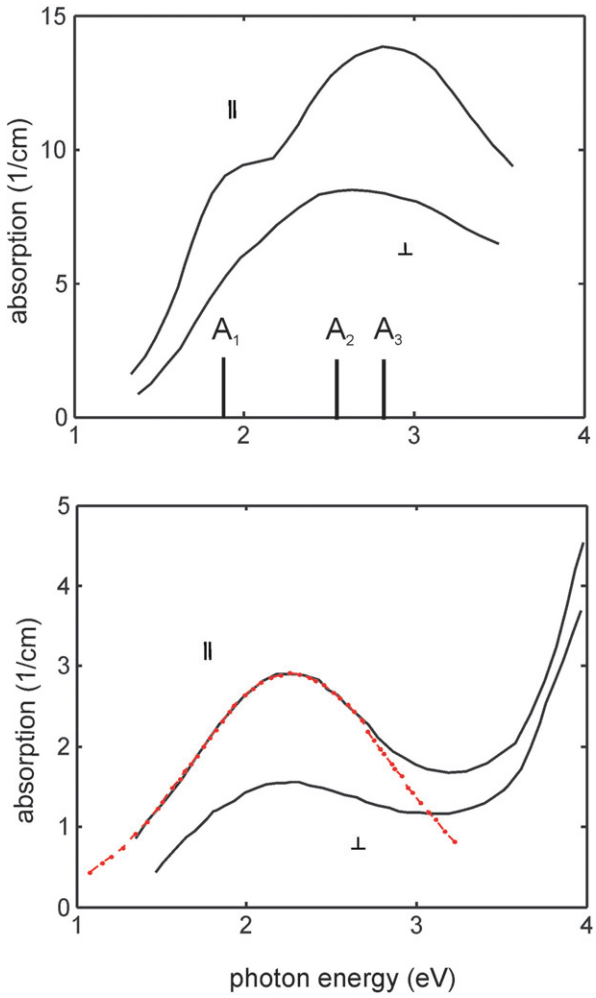

Figure 18. Optical absorption spectra of smoky quartz (upper part) (taken from [48]) and quartz containing Ge (lower part) [49]. The directions of the polarization with respect to the crystal axis are indicated. For Ge-doped quartz the interpretation on the basis of equation (17) is indicated by the dashed line. For details see the text.

experimental ratio $W^2/M = 0.12$ eV of the A_3 band supports a polaron transition between equivalent sites as its origin. This assignment of the A_3 absorption is corroborated by recent quantum chemical calculations by To *et al* [7] and by Shluger *et al* [51]. No excited state tunnelling splitting into two bands, typical for an ideal tetrahedral environment, is observed, however. This may be explained by the slight deviation of the SiO_4 subunit, and thus also of AlO_4, from tetrahedral symmetry already in the quartz host. This is accentuated by the fact that the O^- 2p ground state orbital does not have an axial σ-type orientation. It thus breaks also the axial symmetry around the bond axes. After excitation of the hole in the distorted geometry the final states are not equivalent any more, and resonance splitting is impeded.

To *et al* [7] and Shluger *et al* [51] come to the conclusion that band A_1 at 1.85 eV is caused by hole transfers from O^- to some next nearest O^{2-} ions. Band A_2, near 2.5 eV, remains unexplained. Perhaps compensating ions near the negatively charged Al acceptor could play a

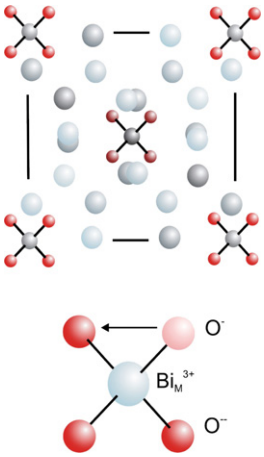

Figure 19. Model of the sillenite crystal structure. Upper part: regular MO_4 tetrahedra (M = Ti, Si or Ge) are located at the centre and the corners of a cube. The further grey to blue balls denote Bi ions that are parts of BiO polyhedra, where the oxygen ions are not shown. The height of these Bi positions is symbolized by the darkness of the colouring: the darker shadings correspond to lower coordinates along an axis perpendicular to the plane. Lower part: Bi_M antisite tetrahedron (Bi_M^{3+}–O_4), with a hole captured at one of the four equivalent oxygen sites. One of the possible small polaron optical transfers is symbolized by the arrow.

role in this context. This is suggested by observations reported by Nassau *et al* [52], indicating that the relative intensities of A_1, A_2 and A_3 depend on the origin and chemical pretreatments of the specimens investigated. Furthermore, findings of Maschmeyer *et al* [53] prove that the A_3 band is not observed, if the oxygen ions around Al^{3+} differ strongly from equivalence by some unidentified local lowering of symmetry. This is the situation found in the citrine variety of quartz and will be discussed in more detail in section 6.

If a hole is captured near Ge^{4+}, no compensation is necessary and, correspondingly, only one band with typical polaron features is observed [49] (peak energy $E_{max} = 2.25$ eV, polaron stabilization $E_P = 0.85$ eV, $W^2/M = 0.17$ eV); figure 18. The value of E_P, less than for SiO_2:Al, is typical for the lower local charge deviation of Ge. Again no excited state splitting is observed. It may be covered by the linewidth or its absence may be caused by the lower than tetrahedral symmetry of the GeO_4 structure, together with the breaking of the axial symmetry by the non-axial O^- ground state.

5.2.2. Sillenites. Ideal MO_4 tetrahedra are building blocks of sillenite crystals, $Bi_{12}MO_{20}$, where M can be any of the cations Ti^{4+}, Si^{4+} and Ge^{4+}; see figure 19. In real specimens of this material, a considerable portion of the M ions are replaced by Bi^{3+}, forming the Bi antisite acceptor [54–56]. Because of the stability of the Bi^{3+} ($6s^2$) configuration, optical ionization will take an electron from one of the four O^{2-} ions [56] rather than from Bi^{3+}, and a bound O^- polaron is formed. This defect offers an example where O^- is formed by direct electron ionization to the conduction band (figure 20). In the paramagnetic state the defect has trigonal, C_{3v}, symmetry, corresponding to localization of the hole at one oxygen site, as proved also by investigations of ultrasound attenuation [19, 20].

Being non-centrosymmetric, space charges induced in a sillenite crystal by inhomogeneous illumination are transposed into refractive index changes via the Pockels effect. This photorefractivity responds rather fast to illumination changes because of the high mobility

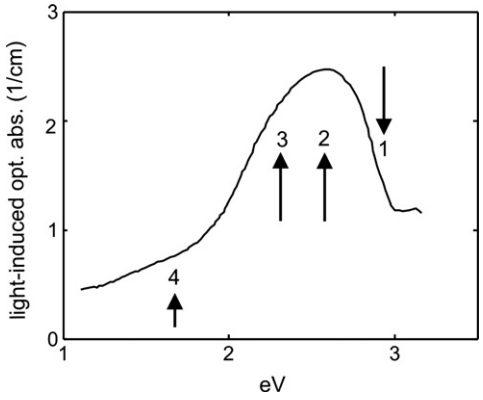

Figure 20. Light induced optical absorption of undoped $Bi_{12}TiO_{20}$ [58]. All numbers refer to figure 21. The arrows 2 and 3 mark bound small polaron transitions in tetrahedral symmetry, resonance split in the excited states. The figure includes the approximate position of the excitation absorption, arrow 1. Since this transition increases the transparency in this energy range, the resulting absorption is decreased. Arrow 4 indicates the increase of absorption by donors filled under illumination.

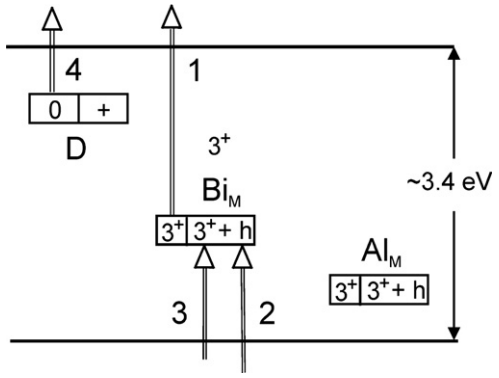

Figure 21. Level scheme comprising the levels of the Bi_M antisite and Al_M defects [56]. A level of a representative donor D is also shown. For the antisite defect the electron excitation, 1, creates the small polaron charge state ($Bi_M^{3+} + h$). The hole excitations 2 and 3 to states resonant with the valence band represent the bound small polaron transitions, split into two bands by excited state resonance. Analogous excitations are also found for Al^{3+}.

of electrons in the conduction band, forming large polarons [57]. The antisite defects and their ionization play an important role in the corresponding charge transfer processes [56]. Figure 21 shows the light induced absorption changes [58] following the excitation labelled '1' in figure 20 and subsequent electron trapping at donors D. A wide band at $M = 2.6$ eV, clearly consisting of two components separated by about 0.3 eV, is seen. This splitting, in the tetrahedral model corresponding to $J \sim 0.10$ eV (figure 8), the value of $E_P = 1$ eV and the W^2/M ratio, 0.14 eV, point to bound hole polaron absorption as its cause. The corresponding transitions 2 and 3 in figure 20 indicate that the (Bi^{3+}–O^-) hole is excited to two tunnelling states (figure 21), which are resonant with the valence band. On its high energy side the light induced absorption band (figure 20) decreases rather abruptly; this is caused by the competition with the superimposed light induced transparency corresponding to process '1' in this energy range (figure 20). At energies lower than about 2 eV, absorptions are seen (in figure 19) which

are attributed to electron excitations '4' (figure 20) at various donors D [56]. These findings indicate that the main intrinsic absorption of the sillenites, causing their typical honey-yellow coloration, is caused by charge transfer excitations of an O^- bound polaron next to Bi_M^{3+} antisite defects [56].

In $Bi_{12}MO_{20}$ melts containing several per cent of Al, instead of the Bi_M^{3+} antisite, an Al_M^{3+} defect forms and the Fermi level is pulled down close to the Al level indicated in figure 21, and the typical antisite coloration is not observed any more. The ionization of the Al^{3+} acceptor, leading to $Al^{3+} + h$, causes an absorption that is almost a replica of the antisite band, now with $M \sim 2.8$ eV. This band certainly is caused by small polaron transitions at the Al–O_4 tetrahedron. Further details about the manifestations of O^- polarons in the sillenites will be published separately.

5.2.3. ZnO. The material crystallizes in the wurtzite structure, in the same way as BeO (section 3.4). Also in ZnO, an O^- polaron bound to the Li acceptor was identified rather early [38]. Recently we found its optical absorption [58], induced by illumination of the material with light energies of the band gap and slightly above (figure 22). A wide band is seen, peaked at ∼1.5 eV. Its appearance is correlated with that of the Li^+–O^- charge state, monitored by means of EPR. Interpreting this band with the theory for tetrahedral polarons (peak at $(8/3)E_P$), a polaron stabilization energy $E_p \sim 0.6$ eV is deduced. This is nearly the same value as that identified for the level of the Li acceptor, $(Li–O)^{-/0}$, 500 to 800 meV above the valence band edge [59]. Apparently, the acceptor depth is strongly influenced by the lattice distortion corresponding to the polaron formation at one oxygen site. It is thus the corresponding sizable lattice coupling of the hole which prevents the substitutional Li_{Zn} acceptor from inducing p-type conductivity in ZnO at room temperature, necessary for use of the material in p–n diodes. It can be remarked that modelling the Li acceptor in ZnO is likely to predict a shallow acceptor level [60] if no provision, see e.g. [7], is made, which allows one to model the hole as localized at one of the four (nearly) equivalent oxygen neighbours of Li.

5.3. Local site symmetries related to octahedral arrangement

5.3.1. Al_2O_3 and $LiNbO_3$. Cox has studied the EPR of O^- defects next to the acceptors V_{Al}, Li_{Al} and Mg_{Al} in Al_2O_3 [61]. A sketch of the configuration of the ground state O^- 2p lobe next to Mg_{Al} within Al_2O_3 is shown in figure 23 [61, 62]. It resembles that of a hole in a cluster of oxygen ions with sixfold cubic arrangement (section 3.3). With Al_2O_3:Mg, an optical absorption band [10] typical for bound hole small polaron absorption has been observed (figure 24). The W^2/M ratio (0.17 eV) of its low energy onset as well as the peak energy near 2.6 eV support this assignment. Interpreting the peak energy on the basis of the prediction for a six-well oxygen cluster (equation (14)), a polaron stabilization energy of $E_P \sim 1.3$ eV is deduced. The asymmetric increase of the absorption on the high energy side of the band peak can, as usual, be attributed to transitions from the O^- ground state to crystal field excited orbitals at the final sites. Al_2O_3:Mg represents a very clear case where the O^- hole is created by doping only and its concentration is increased by annealing in oxidizing atmospheres [10].

The crystal structure of $LiNbO_3$ is closely related to that of Al_2O_3; figure 23. It differs, however, in its tendency to incorporate a sizable non-stoichiometric Li deficit, amounting to about 1% (see, e.g., [63]) in its congruently melting composition. This leads to the formation of Li vacancies, V_{Li}, as intrinsic acceptors, compensated by Nb_{Li} antisite defects as the natural intrinsic donors [64]. O^- holes, probably bound to V_{Li}, have been produced by e-irradiation [65] as well as by two-quantum excitations of valence band electrons to the conduction band [66, 67]. For various reasons, the structure of the defects 'O^- ion next to V_{Li}'

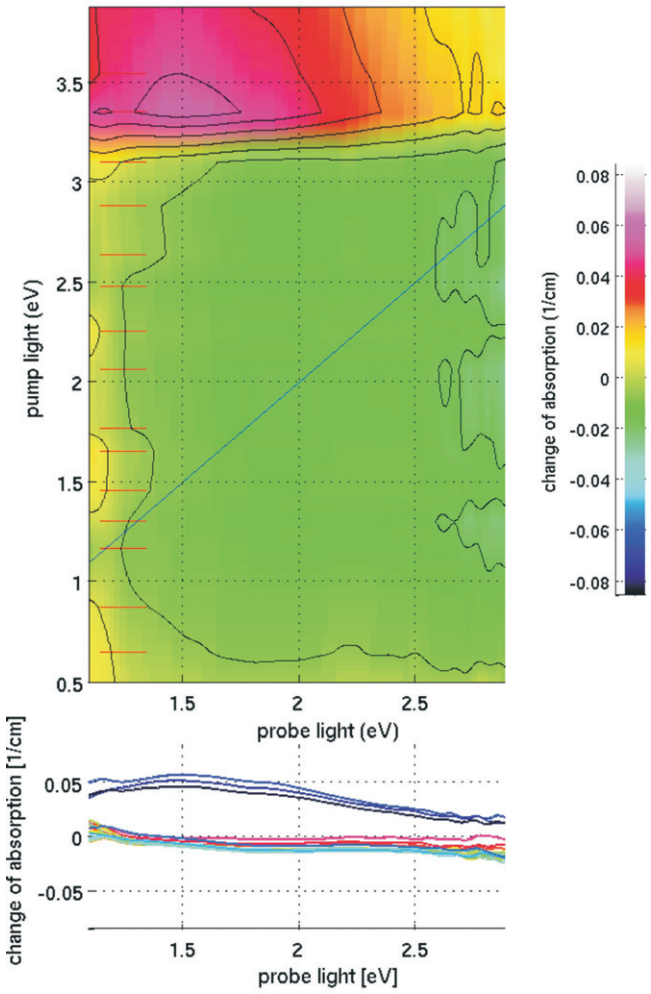

Figure 22. Light induced optical absorption changes of ZnO:Li (6000 ppm) at 12 K [58]. Lower part: changes of absorption curves with energy of exciting light as parameters (not shown). The polarization of the light induced absorption was not studied. Upper part: dependence on the excitation energy included as the ordinate. The increase of absorption, when the energy of exciting light reaches the band gap (∼3.2 eV), is evident. The EPR signal of O^- next to Li increases in parallel.

has not been clarified definitely. By analogy to Al_2O_3 a similar hole configuration is likely to be also present (figure 23). This is supported by the quite comparable optical absorption induced by e-irradiation [65]. Its peak lies near 2.4 eV, corresponding to a polaron stabilization energy close to 1.2 eV. The W^2/M ratio, 0.12 eV, lies in the expected range. It is remarkable that under e-irradiation [65] one of the predominant EPR signals is that of isolated O^-, whereas under two-quantum excitation, O^- as well as Nb_{Li}^{4+} EPR is observed [66, 67]. It originates from a conduction band electron being trapped at a Nb_{Li}^{5+} antisite defect. Accordingly, a broad band with maximum near 1.6 eV, characteristic for Nb_{Li}^{4+} [64], is then superimposed on that of the bound hole polaron.

It is known that $LiNbO_3$ is a very versatile material, employed e.g. in electro-optic and especially photorefractive applications. Besides the hole polaron bound to V_{Li} three further,

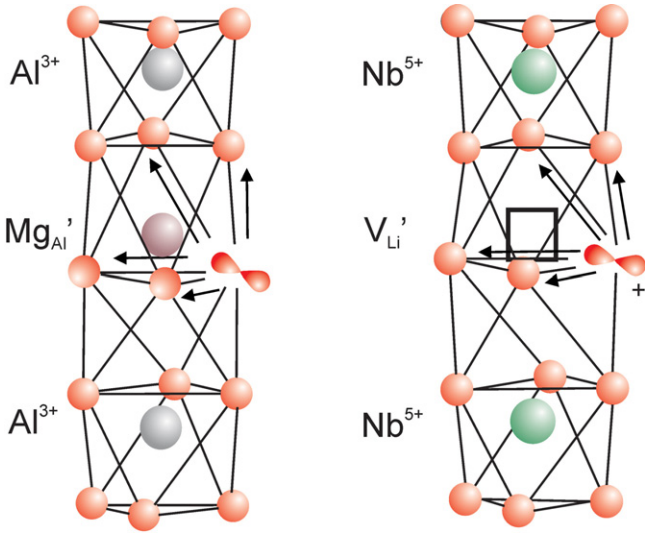

Figure 23. Left: scheme of the O^- defect bound in Al_2O_3 to Mg'_{Al}. Right: model of O^- next to V'_{Li} in $LiNbO_3$, inferred from that of Al_2O_3:Mg through the similarity of the crystal structures.

electronic polaronic structures are involved in the photorefractive behaviour of $LiNbO_3$: the free Nb^{5+}_{Nb} small (to intermediate) polaron, the Nb^{4+}_{Li} electron bound to the antisite defect and the Nb^{4+}_{Li}–Nb^{4+}_{Nb} bipolaron [64, 68].

5.3.2. Topaz. A detailed EPR investigation of topaz [69], aluminium fluorine silicate ($Al_2SiO_4(F, OH)_2$), has revealed that an O^- defect occurs in a crystalline environment as sketched in figure 25 after neutron irradiation. The EPR of this defect is characterized by hyperfine interaction with two equivalent Al nuclei, as shown. It is assumed that the O^- ion is produced from $(OH)^-$ originally present at this site, by neutron irradiation [69]. Under the conditions leading to the EPR of O^- the optical absorption in figure 26 is also observed. Its features ($M = 2$ eV, $W^2/M = 0.10$) suggest ascribing it to a polaron transition as indicated by the weak arrow in figure 25; under illumination the hole is transferred to one of the neighbouring, nearly octahedrally arranged O^{2-} ions. This band, together with the further irradiation induced absorption at 410 nm and that rising below 350 nm, appears to be responsible for the blue coloration of topaz [70]. The additional bands might be caused by transitions to less equivalent oxygen sites near O^- (see section 6).

5.4. Materials with indications for further O^- bound polaron absorptions

Optical absorptions of bound O^- polarons have been identified in a series of further materials, as revealed by the correlation of O^- EPR with absorption bands having features characteristic for polaron absorptions. They are listed here with a few comments, otherwise referring to the related literature.

Under illumination the laser host $YAlO_3$ [71] shows EPR of O^-, which can possibly be assigned to a hole trapped at an oxygen ion next to an Y vacancy. The O^- concentration is proportional to the intensity of an optical absorption band peaked at $M = 1.83$ eV. Its value of W^2/M, 0.12 eV, supports the assignment to bound small polaron absorption.

Stevens *et al* [72] have identified O^- next to a Si^{4+} ion on a P^{5+} site in the non-linear optic material $KTiOPO_4$ (KTP) and an accompanying absorption band with $M = 2.5$ eV

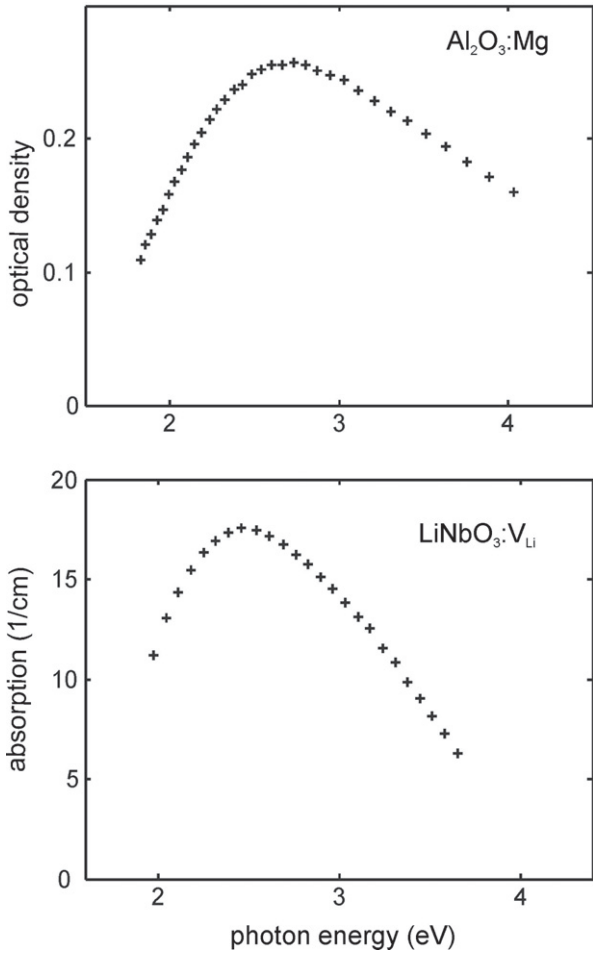

Figure 24. Upper part: optical absorption spectrum of Al_2O_3:Mg, annealed at 1500 °C for 24 h under 10 Pa oxygen pressure, as adapted from [10]. With such a sample, the EPR of the O^- defect sketched in figure 22 is observed. Both optical absorption and EPR intensity increase strongly, if the oxygen pressure is raised. The left half of the absorption band corresponds to $W^2/M = 0.17$ eV. Lower part: optical absorption of congruently melting $LiNbO_3$, irradiated with 1.7 MeV electrons at 77 K, adapted from [65]. The dominating EPR signal is that of O^-, possibly arising from a hole next to V_{Li} ($W^2/M = 0.12$).

and $W^2/M = 0.16$ eV. Both the EPR and the optical features occur after x-irradiation or illumination with 355 nm laser pulses.

In the scheelite $CaWO_4$ a hole, induced by x-irradiation, is found to be trapped near one of the tetrahedrally equivalent oxygen ions next to W^{6+} [73]. This hole localization is stable below 125 K. The authors succeeded in extracting the absorption caused by O^- from the total irradiation induced wide absorption features. A band with $M = 1.7$ eV, slightly depending on the polarization with respect to the crystal axes, was identified. This absorption was attributed to bound O^- small polarons by the authors [73]. Its W^2/M, 0.12 eV, is in favour of this assignment.

Optical absorption with $M = 1.5$ eV, $W^2/M = 0.11$ eV, is found to arise in $KTaO_3$ simultaneously with the EPR of an illumination induced O^- bound hole [74]. The correlation

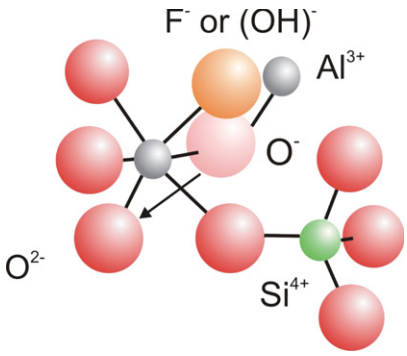

Figure 25. A section of a topaz crystal structure, according to [69] containing O^- on an OH^- site before neutron irradiation. There are four rather equivalent oxygen ions next to O^-. One of the possible light induced hole polaron transfers is symbolized by a thin arrow.

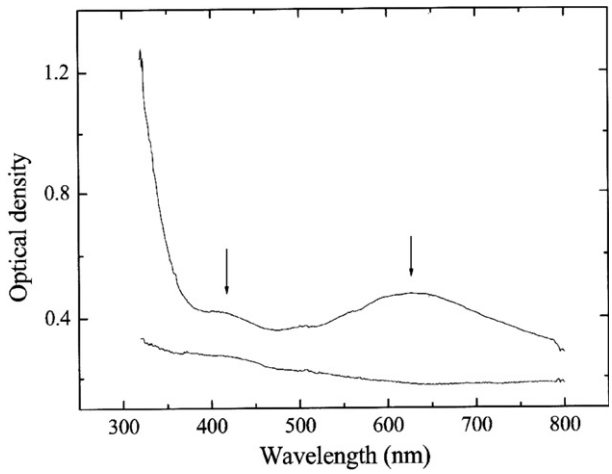

Figure 26. Optical density induced in topaz by n-irradiation [70], upper trace, in comparison to that for an unirradiated reference sample, lower trace. The band with peak at the right arrow ($M = 2.0$ eV) has a value $W^2/M = 0.10$, typical for bound small polaron absorption.

between EPR and optical absorption was also established by ODMR studies [31]. The acceptor defect binding the hole cannot yet be identified.

For lithium tetraborate ($Li_2B_4O_7$) Malovichko *et al* [75] have identified a series of paramagnetic defects, induced by fast neutrons, which can partly be attributed to O^-. Among the simultaneously occurring absorption bands there are some with $M \sim 2.5$ eV and $W^2/M = 0.11$ eV.

X-irradiation induces O^- EPR in Y- or Ca-stabilized zirconia (YSZ or CaSZ), as found by Orera *et al* [76]; these centres are connected with an optical absorption band with $M = 2.6$ eV and $W^2/M = 0.17$ eV.

It is likely that this list of examples is not exhaustive. In many cases the O^- defects mentioned and the related optical absorptions are stable only at low temperatures. With rising temperature they tend to decay by recombination with the compensating electrons. In some cases the primary O^- defects appear to be precursors for defects causing permanent absorption bands.

6. Bound O^- but no typical polaron absorption

Several examples are known where EPR characteristic for a hole localized at one oxygen site is observed but where the correlated optical absorption is not typical for bound small polarons. How do these cases fit into the present context?

The first such defect concerns the natural citrine modification of quartz, not to be confused with the citrine variety which results from annealing amethyst [53]. Just like smoky quartz, citrine also shows EPR of O^- at one site next to Al^{3+}. Instead of a typical bound polaron band, however, an absorption starting at slightly higher energies than for smoky quartz (figure 18) and strongly rising towards shorter wavelengths is observed. It is satisfying in this situation that the oxygen ions next to Al^{3+} are found not to be equivalent to each other [53]; this is caused apparently by some associated further defect ion, strongly favouring only one single oxygen ion next to Al^{3+} to trap the hole. Thus the precondition for the appearance of ideal bound small polaron absorption is not fulfilled. Since it takes more energy now to transfer the hole to an energetically less favourable oxygen neighbour, the onset of the transition energy will be higher, as implied by figure 16.

A situation similar to that for citrine is also identified for the mineral brazilianite ($NaAl_3(OH)_4(PO_4)_2$). Here the O^- ion, carrying the hole, is locked between Al^{3+} and P^{5+} and no equivalent oxygen ions are nearby [77]. Therefore the characteristic bound polaron absorption does not occur.

The yellow colour of tourmaline was established by very detailed EPR, ODMR and optical absorption investigations [78] to be caused by transitions from an O^- ground state. However, it is not the typical bound polaron absorption that is correlated to the O^- EPR but a band peaked at 3.4 eV (and a further one at 5.1 eV), having its onset in the blue range of the visible; this causes the yellow colour. The rather low value of W^2/M determined, 0.04, as well as the appearance of two bands, also argue against inequivalent oxygen ions as final transfer sites.

Finally the case of lithium triborate, LiB_3O_5, x-irradiated at 77 K [79, 80], is discussed. It contains O^- holes at single oxygen sites and an optical absorption band with peak at 4.1 eV. The compensating electron, trapped at a B^{3+} ion of the lattice, is also identified. Both defects become unstable near 125 K, and their joint recombination causes photoluminescence. The position and width of the absorption band are not characteristic for a bound hole polaron. Indeed, the strongest overlap of the hole ground state 2p lobe is with non-equivalent oxygen ions. The most effective light induced optical transfer is expected to occur along the direction having the strongest overlap to the final site, here not an equivalent one. This would raise the O^- hole transfer absorption to energies higher than for equivalent oxygen ions. The 4.1 eV optical band could alternatively be caused by the boron electron trap.

7. Materials with paramagnetic cations

7.1. NiO:Li

The similarity of this system to MgO:Li is evident: both materials crystallize in the rocksalt structure, and Li tends to be compensated by O^- holes. Since, in contrast to Mg^{2+}, Ni^{2+} has an open shell structure ($3d^8$, spin $S = 1$), the question could arise of whether here the hole rather forms Ni^{3+} ($3d^7$). Electron emission studies by van Elp *et al* [81] have decided this issue, revealing that in NiO:Li also the hole resides mainly at the oxygen ions next to Li. It was even established that the sign of the transfer energy, J, is identical to that found for MgO:Li (figure 4), putting the Γ_3 (O_h) ground state lowest. It remained to find out, however, whether the hole is localized at one site as a small polaron. Quantum chemical studies by Mackrodt *et al* [82] indicated that this appears indeed to be the case.

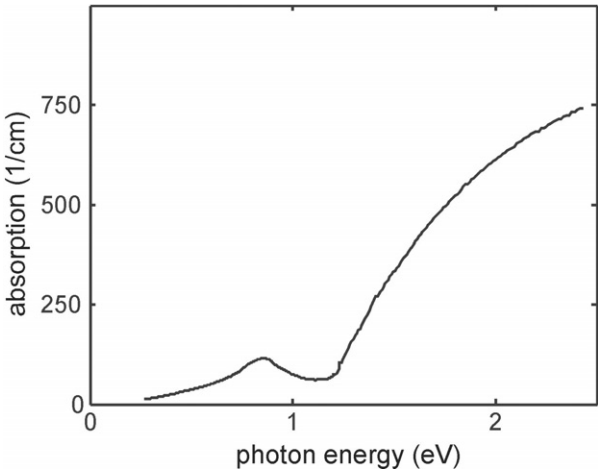

Figure 27. Frequency dependence of the absorption of NiO:Li (3000 ppm), measured at 100 K. The graph was calculated from the real part of the conductivity reported in [83], assuming a refractive index $n = 1.5$ for the given energy range. The absorption feature around 0.8 eV was attributed to free hole small polarons in [83].

Therefore, one expects to observe absorption spectra resembling those of MgO:Li. Optical investigations of NiO:Li were published rather early by Austin *et al* [83], and these authors pointed out that a strong Li induced extinction does indeed occur especially strongly at energies above ∼1 eV. Figure 27 shows the relevant portions of data published by Austin *et al* [83]. Their measurements extended from the far infrared region up to 2.5 eV. Shown (figure 27) are the data obtained with NiO:Li from which the large background absorptions of undoped NiO, resulting from the d–d and charge transfer transitions of Ni^{2+}, have been subtracted. Such differences between very large numbers are certainly connected with sizable errors. At present, therefore, it can only be stated that O^- bound polaron absorption appears to occur in the expected energy range, but it cannot be decided whether NiO:Li conforms with the details predicted by theory. In contrast to the situation for MgO:Li, the exchange interaction of the O^- hole with the surrounding Ni^{2+} ions could also influence the optical properties. In any case, the NiO:Li system appears to be ideal for studying the properties of bound hole polarons in a magnetic environment. The absorption feature with maximum at 0.8 eV in figure 27 was shown to exhibit features expected for thermally excited free hole polarons [83]. No explanation was offered then for the strong, Li induced extra absorption at higher energies, treated here. Unfortunately the absorption at energies above 2.5 eV, where the peak position of O^- bound polaron absorption can be expected, was not studied [83].

7.2. $LaMnO_3$:Sr

The introduction of Sr^{2+} on the Mn^{3+} ($3d^4$) site creates acceptors in this perovskite material, capable of exhibiting colossal magnetoresistance, and correspondingly also here the question is discussed (see, e.g., [84]) of whether the compensating holes form Mn^{4+} ($3d^3$, $S = 3/2$) or rather O^- ions, possibly bound to the acceptor ion. Electron energy loss spectra [85] indicate that the holes introduced have strong oxygen character, and at low temperatures and for low Sr dopings ($x \leqslant 0.14$) the material is insulating [85], excluding free holes. Furthermore, x-emission studies [86] show that for $x < 0.18$ the Mn valency is not changed by Sr doping. In this situation it is not unexpected that optical absorption of such material [87] has features

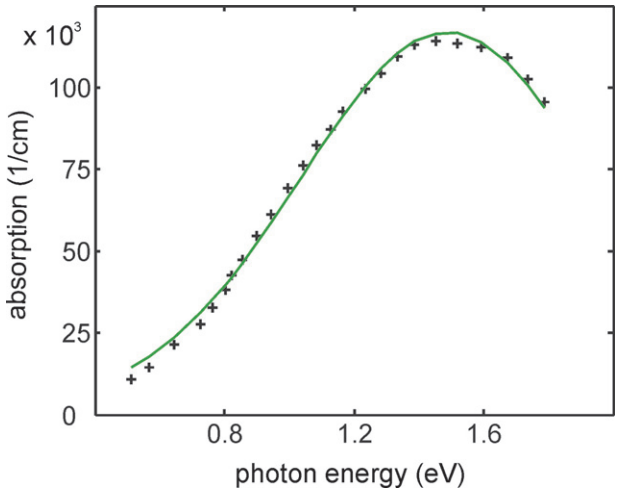

Figure 28. Optical absorption of $La_{0.875}Sr_{0.125}MnO_3$ at 250 K, as adapted from [87]. The full line shows the interpretation of the data with equation (17), using $\hbar\omega_0 = 0.12$ eV, $E_P = 1.6$ eV.

typical for O^- holes bound to the Sr acceptor (figure 28), similar to the case for O^- next to Na in $BaTiO_3$.

The measured value $W^2/M = 0.17$ eV is typical for an O^- bound polaron transition. Influences of exchange coupling with the magnetic Mn ions of the host cannot be excluded.

The prototypes of oxide materials containing holes induced by acceptor doping in an environment of paramagnetic cations are the cuprate superconductors, e.g. $La_{1-x}Sr_xCuO_4$. One might expect here holes also to be bound to the Sr acceptor, yielding related optical features. In the optical absorption spectra of $La_{1-x}Sr_xCuO_4$ [88], however, no clear indication of bands is found which could be assigned to this situation. In contrast, starting at low Sr concentrations, at first a wide optical band ('mid-infrared band') with a peak at 0.5 eV occurs, which could be attributed to free small polaron optical absorption. For light induced phenomena of this type, see [89]. With rising Sr doping, features at lower energies, caused by free holes with weaker coupling to the lattice, are identified. It appears that, because of the strong Cu^{2+}–O^{2-} covalency, it is more favourable that the holes move freely in the Cu–O planes rather than being localized next to the acceptors. The appearance of the free small polaron-type absorption at low Sr concentration appears to be favoured by doping induced lattice disorder. This is also supported by the relative increase of the 0.5 eV band in structurally perturbed material, such as with thin evaporated $La_{1-x}Sr_xCuO_4$ layers [90].

8. Concluding remarks

It was shown that the model 'hole trapped at one of several equivalent oxygen ions next to an acceptor defect' describes a typical situation found in numerous oxide materials; it is characterized by strong optical absorptions with wide bands extending into the visible. These phenomena are based on the stabilization of holes as small polarons by about 1 eV, once a defect induced localization at one oxygen site has taken place. Such bound O^- polarons play essential roles in various functions of oxide materials: radiation or illumination induced absorptions, catalysis, coloration of gemstones, photorefractivity, etc. In experiments investigating the light induced charge transfer paths of carriers in oxide materials, the established characteristic optical

fingerprints of O^- bound polarons are useful for identifying hole processes by optical means only (see e.g. [91]).

There are various fields of phenomena which touch on the presented domain of O^- bound polarons. First we make some further remarks on the relationship to free small polarons, beyond those mentioned above. The properties of small polarons in general are essentially determined by their localization at one site. For bound polarons the issue is clearly decided by the strong lattice couplings, clearly dominating their tunnelling among the equivalent sites. This is less pronounced for free holes; their transfer from site to site is stronger, and it is unlikely that free small oxygen hole polarons exist. Objects displaying the corresponding experimental features may rather be induced by lattice irregularities, triggering the carrier localization. It is then rather a matter of semantics whether these objects should be called free small polarons. Conduction bands of transition metal oxides tend to be narrower than the valence bands. Therefore the chances are higher that free electron small polarons might form. It was shown, however, that even for $BaTiO_3$, EPR signals pointing to free small Ti^{3+} polarons are also rather induced by lattice irregularities [92].

Next, it is appropriate to compare the theoretical approach employed in this overview with alternative methods. Here it was possible to collect the numerous manifestations of bound small O^- polarons in various oxide compounds under a common guideline by using the presented unifying configuration coordinate model. This also allowed us to model special traits of such objects, such as the dependence of the absorption features on the topology of the defects and their excited state splittings. The simplicity of the model is the prerequisite for the generality of the results obtained, applicable to a large class of compounds: besides a low number of phenomenological parameters, it uses only the symmetry of the lattice distortion fields occurring. In reality the latter are represented by the collective position changes of the electrons and ions in clusters of many particles (see, e.g., Shluger *et al* [93]). If it is not generality of the results achieved that is intended, more detailed information on many properties of bound polarons can be obtained by quantum chemical simulations of such defects. These methods can alternatively lead to rather detailed insights into the microscopic structure of the defects and the straightforward prediction of quantities such as the 'small polaron' optical absorption transitions, the polaron energies or the levels of the acceptors, to which a polaron is bound. For recent examples see, e.g., [7].

Of course, the stabilization of holes at one ion site next to an acceptor defect is not restricted to oxide materials. Holes of this type have also been identified, e.g., in sulfides and selenides. The defect which was most intensively investigated in this context is Se^- at a single Se site next to the Zn vacancy in ZnSe. This was modelled quantum chemically by Harding and Stoneham [94] and investigated experimentally as well as interpreted phenomenologically by Watkins *et al* as reported in a series of papers culminating in an ODMR by MCD study of the optical absorption of the defect [41]. Numerous similarities to the O^- bound polarons summarized in the present review were identified. The optical absorption of S^- holes next to V_{Zn}–Cl associates in ZnS has been found to have typical polaron absorption bands peaked at 1.8 eV [95]. Strong optical absorptions connected with S^- typical EPR have also been identified in the photorefractive material $Sn_2P_2S_6$ [96] after illumination.

So far, only single hole polarons at one site have been treated. Interactions between polarons have become important manifestations of such carriers in the last few decades. We shall first deal with pairs of polarons bound to one acceptor defect. There are numerous cases of this type, e.g. two holes bound to V_{Mg} in MgO [97] or to V_{Al} in Al_2O_3 [61] and to related defects [97]. The exchange interaction between the holes leads to singlet ($S = 0$) or triplet ($S = 1$) states. Experimentally it is found that in these cases $S = 0$ is only slightly favoured as the ground state. The surprisingly low energy of excitation to $S = 1$ has been accounted for by

Stoneham *et al* [97] by invoking an admixture of O^0–O^{2-}-type excited states by configuration interaction to the main configuration O^-–O^-. In favourable cases this mechanism could even lead to a ferromagnetic, $S = 1$, ground state. At least for the case V^0, i.e. for two holes bound to V_{Mg} in MgO, the optical absorption is quite similar to the one-hole case, V^- [33]. So also for V^0 the optically induced transfer of a single hole between equivalent oxygen ligands is active.

It is beyond the scope of the present review, which is focused on bound single polarons, to dwell on phenomena based on the interaction of free polarons, such as the formation of free bipolarons and their possible roles in superconductivity (see, e.g., [98]) and colossal magnetoresistance (e.g., [99]). The present results on a large variety of bound polarons in numerous compounds may, however, have a fruitful bearing also for the cases of interacting free polarons.

Acknowledgments

I thank A M Stoneham for useful hints concerning the scope of the review, A L Shluger for a discussion and Th W Kool for critically reading the manuscript.

References

[1] Emin D 1993 *Phys. Rev.* B **48** 13691
[2] Alexandrov A S, Kabanov V V and Ray D K 1994 *Physica* C **224** 227
[3] Reik H G 1963 *Solid State Commun.* **1** 67
[4] Klinger M I 1963 *Phys. Lett.* **7** 102
[5] Reik H G and Heese D 1967 *J. Phys. Chem. Solids* **28** 581
[6] Norgett M J, Stoneham A M and Pathak A P 1977 *J. Phys.: Solid State Phys.* **10** 555
[7] To J, Sokol A A, French S A, Katsoyannis N and Catlow C R A 2005 *J. Chem. Phys.* **122** 144704
[8] Shluger A L and Stoneham A M 1993 *J. Phys.: Condens. Matter* **5** 3049
[9] Calvani P 2001 *Riv. Nuovo Cimento* **24** 1
[10] Wang H A, Lee C H, Kröger F A and Cox R T 1983 *Phys. Rev.* B **27** 3821
[11] Weil J A, Bolton J R and Wertz J E 1994 *Electron Paramagnetic Resonance* (New York: Wiley) p 100
[12] Maiwald M and Schirmer O F 2003 *Europhys. Lett.* **64** 776
[13] Possenriede E, Jacobs P and Schirmer O F 1992 *J. Phys.: Condens. Matter* **4** 4719
[14] Donnerberg H, Többen S and Birkholz A 1997 *J. Phys.: Condens. Matter* **9** 6359
[15] Spaeth J M, Niklas J R and Bartram R H 1992 *Structural Analysis of Point Defects in Solids* (Berlin: Springer)
[16] Izen E H, Mazo R M and Kemp J C 1973 *J. Phys. Chem. Solids* **34** 1431
[17] Meyer M, Schirmer O F and Pankrath R 2004 *Appl. Phys.* B **79** 395
[18] van den Brom W E and Volger J 1974 *Physica* **7** 245
[19] Rehwald W, Frick K, Lang G K and Meier E 1976 *J. Appl. Phys.* **47** 1292
[20] Grewal P K and Lea M J 1983 *J. Phys. C: Solid State Phys.* **16** 247
[21] Fowler W B 1968 *Physics of Color Centers* ed W B Fowler (New York: Academic) p 59
[22] Gebhardt W and Kühnert H 1964 *Phys. Lett.* **11** 15
[23] Lax M J 1952 *Chem. Phys.* **20** 1752
[24] Schirmer O F, Koidl P and Reik H G 1974 *Phys. Status Solidi* b **62** 385
[25] Eagles D M 1963 *Phys. Rev.* **130** 1381
[26] Schirmer O F 1976 *Z. Phys.* B **24** 235
[27] Rose B H and Cowan D L 1974 *Solid State Commun.* **15** 775
[28] Henderson B 1976 *J. Phys. C: Solid State Phys.* **9** L579
[29] Chen Y and Sibley W A 1967 *Phys. Rev.* **154** 842
[30] Rius G, Hervé A, Picard R and Santier C 1976 *J. Physique* **37** 129
[31] Pape M 2004 *Doctoral Thesis* Osnabrück
[32] Henderson W and Wertz J E 1977 *Defects in the Alkaline Earth Oxides* (London: Taylor and Francis) p 60
[33] Kappers L A, Dravnieks F and Wertz J E 1974 *J. Phys. C: Solid State Phys.* **7** 1387
[34] Harding J H 1979 *J. Phys. C: Solid State Phys.* **12** 3931
[35] Abraham M M, Chen Y, Boatner L A and Reynolds R W 1976 *Phys. Rev. Lett.* **37** 849
[36] Catlow C R A, French S A, Sokol A A and Thomas J M 2005 *Phil. Trans. R. Soc.* A **363** 913

[37] Schirmer O F and Schnadt R 1976 *Solid State Commun.* **18** 1345
[38] Schirmer O F 1968 *J. Phys. Chem. Solids* **29** 1407
[39] Schirmer O F 1978 *J. Phys. C: Solid State Phys.* **11** L65
[40] Varnhorst T, Schirmer O F, Kröse H, Scharfschwerdt R and Kool Th W 1996 *Phys. Rev.* B **53** 116
[41] Jeon D Y, Gislason H P and Watkins G D 1993 *Phys. Rev.* B **48** 7872
[42] Austin I G and Mott N F 1969 *Adv. Phys.* **18** 41
[43] Bartram R H, Swenberg C E J and Fournier T 1965 *Phys. Rev.* **139** A941
[44] Hayes W and Stoneham A M 1985 *Defects and Defect Processes in Nonmetallic Solids* (New York: Wiley)
[45] for an overview see Weil J A 1975 *Radiat. Eff.* **26** 261
[46] Hayes W and Jenkin T J 1986 *J. Phys. C: Solid State Phys.* **19** 6211
[47] Schnadt R and Schneider J 1979 *Phys. Kondens. Materie* **11** 19
[48] Schirmer O F 1976 *Solid State Commun.* **18** 1349
[49] Jenkin T J L, Koppitz J, Schirmer O F and Hayes W 1987 *J. Phys. C:Solid State Phys.* **20** L367
[50] Meyer B K, Lohse F, Spaeth J M and Weil J A 1984 *J. Phys. C: Solid State Phys.* **17** L31
[51] Shluger A L 2006 private communication
[52] Nassau K and Prescott B E 1975 *Phys. Status Solidi* a **29** 659
[53] Maschmeyer D, Niemann K, Hake H, Lehmann G and Räuber A 1980 *Phys. Chem. Minerals* **6** 145
[54] Briat B, Hamri A, Romanov N V, Ramaz F, Launay J C, Thiemann O and Reyher H J 1995 *J. Phys.: Condens. Matter* **7** 6951
[55] Reyher H J, Hellwig U and Thiemann O 1993 *Phys. Rev.* B **47** 5638
[56] Briat B, Grachev V G, Malovichko G I, Schirmer O F and Wöhlecke M 2006 *Photorefractive Materials and Their Applications* vol 2, ed P Günter and J P Huignard (Berlin: Springer) at press
[57] Biaggio I, Hellwarth R W and Partanen J P 1997 *Phys. Rev. Lett.* **78** 891
[58] Wykhoff J and Schirmer O F, unpublished
[59] Meyer B K, Alves H, Hofmann D M, Kriegseis W, Forster D, Bertram F, Christen J, Hoffmann A, Straßburg M, Dworzak M, Haboeck U and Rodina A V 2004 *Phys. Status Solidi* b **244** 231
[60] Wardle M G, Goss J P and Briddon P R 2005 *Phys. Rev.* B **71** 155205
[61] Cox R T 1971 *Solid State Commun.* **9** 1989
[62] Adrian F J, Jette A N and Spaeth J M 1985 *Phys. Rev.* B **31** 3923
[63] Räuber A 1978 *Current Topics in Materials Science* vol 1, ed E Kaldis (Amsterdam: North-Holland) p 48
[64] Schirmer O F, Thiemann O and Wöhlecke M 1991 *J. Phys. Chem. Solids* **52** 185
[65] Halliburton L E, Sweeney K L and Chen C Y 1984 *Nucl. Instrum. Methods Phys. Res.* B **1** 344
[66] Schirmer O F and von der Linde D 1978 *Appl. Phys. Lett.* **33** 35
[67] von der Linde D, Schirmer O F and Kurz H 1978 *Appl. Phys.* **15** 153
[68] Herth P, Granzow T, Schaniel D, Woike T, Imlau M and Krätzig E 2005 *Phys. Rev. Lett.* **95** 067404
[69] da Silva D N, Guedes K J, Pinheiro M V B, Gaedes K J, Spaeth J M and Krambrock K 2005 *Phys. Chem. Minerals* **32** 436
[70] da Silva D N, Guedes K J, Pinheiro M V B, Gaedes K J, Spaeth J M and Krambrock K 2005 *Phys. Status Solidi* c **2** 397
[71] Schirmer O F, Blazey K W, Berlinger W and Diehl R 1976 *Phys. Rev.* B **11** 4201
[72] Stevens K T, Setzler S D, Halliburton L E, Scripsick M P and Rottenberg J 1999 *J. Appl. Phys.* **85** 1063
[73] Herget M, Hofstaetter A, Nickel T and Scharmann A 1987 *Phys. Status Solidi* b **14** 523
[74] Maiwald M 1999 *Doctoral Thesis* Osnabrück
[75] Malovichko G I, Grachev V G and Matkovskii A O 1991 *Sov. Phys.—Solid State* **33** 1107
Malovichko G I, Vitruk L E and Yurchenko N Yu 1992 *Sov. Phys.—Solid State* **34** 272
[76] Orera V M, Merino R I, Chen Y, Cases R and Alonso P J 1990 *Phys. Rev.* B **42** 9782
[77] Lehmann G 1978 *Angew. Chem. Int. Edn Engl.* **17** 89
[78] Krambrock K, Pinheiro M V B, Gaedes K J, Medeiros S M, Schweizer S and Spaeth J M 2004 *Phys. Chem. Minerals* **31** 168
[79] Wei H, Chirila M M, Garces N Y, Halliburton L E, Lupinski D and Villeval P 2003 *Phys. Rev.* B **68** 094111
[80] Scripsick M P, Fang X H, Edwards C J, Halliburton L E and Tyminski J K 1993 *J. Appl. Phys.* **19** 6211
[81] van Elp J, Eskes H, Kuiper P and Sawatzky G A 1992 *Phys. Rev.* B **45** 1612
[82] Mackrodt W C and Middlemiss D S 2003 *J. Phys.: Condens. Matter* **16** S2911
[83] Austin I G, Clay B D and Turner C E 1968 *J. Phys. C: Solid State Phys. (Proc. Phys. Soc.) Ser. 2* **1** 1418
[84] Kovaleva N N, Gavertin J L, Shluger A L, Boris A V and Stoneham A M 2002 *J. Exp. Theor. Phys.* **94** 178
[85] Ju H L, Sohn H C and Krishnan K M 1997 *Phys. Rev. Lett.* **79** 3230
[86] Galakov V R, Demeter M, Bartkowski S, Neumann M, Ovechkina N A, Kurmaev E Z, Lobachevskaya N I, Mukovskii Ya M, Mitchell J and Ederer D L 2002 *Phys. Rev.* B **65** 113102

[87] Mayr F, Hartinger C, Paraskevopoulos M, Pimenov A, Hemberger J, Loidl A, Mukhin A A and Balbashov A M 2000 *Phys. Rev.* B **62** 15673
[88] Uchida S, Ido T, Takagi H, Arima T, Tokura Y and Tajima S 1991 *Phys. Rev.* B **43** 7942
[89] Mihailovic D, Foster C M, Voss K and Heeger A J 1990 *Phys. Rev.* B **42** 7898
[90] Wahlbrink T 2001 *Doctoral Thesis* Osnabrück
[91] Scharfschwerdt R, Schirmer O F, Hesse H and Rytz D 1999 *Appl. Phys.* B **68** 807
[92] Lenjer S, Schirmer O F, Hesse H and Kool Th W 2002 *Phys. Rev.* B **66** 165106
[93] Shluger A L, Heifets E N, Gale J D and Catlow C R A 1992 *J. Phys.: Condens. Matter* **4** 5711
[94] Harding J H and Stoneham A M 1982 *J. Phys. C: Solid State Phys.* **15** 4649
[95] Schneider J, Dischler B and Räuber A 1970 *J. Phys. Chem. Solids* **31** 337
[96] Ruediger A, Schirmer O, Odoulov S, Shumelyuk A and Grabar A 2001 *Opt. Mater.* **18** 123
[97] Stoneham A M, Pathak A P and Bartram R H 1976 *J. Phys. C: Solid State Phys.* **9** 73
[98] Alexandrov A S and Mott N F 1994 *Rep. Prog. Phys.* **57** 1197
[99] Alexandrov A S and Bratkovsky A M 1998 *Phys. Rev. Lett.* **82** 141